Algebraic Bethe ansatz and tensor networks

V. Murg,[1] V. E. Korepin,[2,*] and F. Verstraete[1]

[1]*Fakultät für Physik, Universität Wien, Boltzmanngasse 3, A-1090 Vienna, Austria*

[2]*C. N. Yang Institute for Theoretical Physics, State University of New York at Stony Brook, Stony Brook, New York 11794-3840, USA*

(Received 16 March 2012; published 20 July 2012)

The algebraic Bethe ansatz is a prosperous and well-established method for solving one-dimensional quantum models exactly. The solution of the complex eigenvalue problem is thereby reduced to the solution of a set of algebraic equations. Whereas the spectrum is usually obtained directly, the eigenstates are available only in terms of complex mathematical expressions. This makes it very hard, in general, to extract properties from the states, for example, correlation functions. In our work, we apply the tools of tensor-network states to describe the eigenstates approximately as matrix product states. From the matrix product state expression, we then obtain observables like the structure factor, dimer-dimer correlation functions, chiral correlation functions, and one-particle Green function directly.

DOI: 10.1103/PhysRevB.86.045125 PACS number(s): 75.10.−b, 05.10.−a, 02.70.−c, 03.67.−a

I. INTRODUCTION

The coordinate Bethe ansatz[1] is an extremely successful method for solving one-dimensional problems exactly. It reduces the complex problem of diagonalizing the Hamiltonian to finding the solutions of a set of algebraic equations. Once solutions to these algebraic equations are found—numerical approaches to find them efficiently exist in many cases—the eigenvalues are known exactly. However, the eigenstates are available only as complex mathematical expressions the structure of which is not evident. This makes it insuperable, in general, to get interesting properties out of the states—like their entanglement characteristics or their correlations. The algebraic Bethe ansatz[2] reveals more about the structure of the eigenstate and offers new perspectives to obtain scalar products,[3] norms,[2] and correlations.[2]

In this paper, we point out this structure by formulating the algebraic Bethe ansatz in the pictoresque tensor network language. The description of states in terms of tensor networks has been very successful in the recent past. One-dimensional matrix product states (MPSs)[4–9] form the basis for the extremely successful density matrix normalization group (DMRG).[10,11] Also, they have attracted considerable interest in the interdisciplinary field of quantum information and condensed matter physics.[6–9] For describing the ground state of systems on higher-dimensional lattices, projected entangled pair states (PEPSs)[12] were introduced and proved to be useful for the numerical study of ground states of two-dimensional systems.[13,14] The multiscale entanglement renormalization ansatz[15,16] allows the description and numerical study of critical systems.

From the tensor network desription of the Bethe eigenstates it is immediately obvious that eigenstates can be described as MPSs[17] (this idea was developed independently by Katsura and Maruyama[18]). Katsura and Maruyama also show that the alternative formulation of the Bethe ansatz by Alcaraz and Lazo 19–21 is equivalent to the algebraic Bethe ansatz.

The tensor-network form of Bethe eigenstates allows us to calculate numerically expectation values of arbitrary observables. This extends previous numerical approaches that focus on two-point correlation functions in systems with periodic boundary conditions.[22] Our approach requires the approximate contraction of a tensor network such as the one depicted in Fig. 1. We achieve this by using a method similar to that for time evolution in the DMRG.[8,23] We show, for the case of the antiferromagnetic Heisenberg model and the *XXZ* model with both periodic and open boundary conditions, that two-point, dimer-dimer, and chiral correlation functions as well as the one-particle Green function can be obtained for 50 sites with an extremely high precision.

The paper is structured as follows: in Sec. II we discuss the tensor-network form of the Bethe ansatz; Sec. III deals with the numerical contraction of this tensor network, and in Sec. IV the results for the correlations of the *XXX* and *XXZ* model are presented. In Appendixes A and B the algebraic Bethe ansatz is described in the picturesque tensor-network language for periodic and open boundary conditions, making evident the tensor-network structure of the Bethe eigenstates.

II. TENSOR-NETWORK FORM OF BETHE SOLUTIONS

Typically, Bethe eigenstates are obtained as products of operators $B(\mu_j)$ applied on a certain vacuum state $|\mathrm{vac}\rangle$, i.e.,

$$|\Psi(\mu_1,\ldots,\mu_M)\rangle = B(\mu_1)\cdots B(\mu_M)|\mathrm{vac}\rangle. \tag{1}$$

The parameters $\{\mu_j\}$ are thereby solutions of Bethe equations and the $B(\mu_j)$ values play the role of creation operators. In the case of the antiferromagnetic Heisenberg model and the *XXZ* model with periodic boundary conditions, the vacuum corresponds to the state with all spins up and each operator $B(\mu_j)$ creates one down-spin. Thus, the product of M such operators applied to the vacuum creates a state with M down-spins, i.e., magnetization $S_z = N/2 - M$ (with N being the number of spins). $B(\lambda)$ is an operator acting on the whole Hilbert space of dimension 2^N, but it has the well-structured form of a matrix product operator (MPO)[24] with virtual dimension 2. Indeed, as shown in Appendix A,

$$B(\lambda) = \sum_{\substack{k_1\cdots k_N \\ l_1\cdots l_N}} \langle 0|\mathcal{L}^{k_1}_{l_1}(\lambda)\cdots\mathcal{L}^{k_N}_{l_N}(\lambda)|1\rangle o^{k_1}_{l_1}\otimes\cdots\otimes o^{k_N}_{l_N},$$

with $k,l\in\{0,1\}$, $o^k_l = |k\rangle\langle l|$ ($0\equiv\uparrow$, $1\equiv\downarrow$), and $\mathcal{L}^k_l(\lambda)$ being 2×2 matrices dependent on the parameter λ. The product of operators $B(\mu_1)\cdots B(\mu_M)$ can be read as the contraction

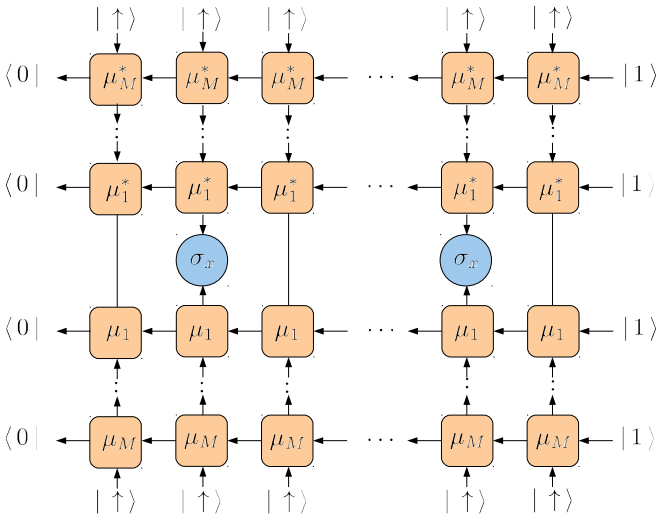

FIG. 1. (Color online) Tensor network describing correlations $\langle\sigma_x^{(i)}\sigma_x^{(j)}\rangle$ with respect to a Bethe eigenstate.

of the set of four-index tensors $[\mathcal{L}_l^k(\mu_j)]_{r'}^r$ with respect to a rectangular grid, as shown in Fig. 2. Thereby, r and r' label the outgoing and incoming horizontal indices, and k and l the outgoing and incoming vertical indices, respectively. Explicitly, the matrices $\mathcal{L}_l^k(\lambda)$ read

$$\mathcal{L}_0^0(\lambda)=\begin{pmatrix}1 & 0\\ 0 & c(\lambda)\end{pmatrix},\quad \mathcal{L}_1^0(\lambda)=\begin{pmatrix}0 & 0\\ b(\lambda) & 0\end{pmatrix},$$
$$\mathcal{L}_0^1(\lambda)=\begin{pmatrix}0 & b(\lambda)\\ 0 & 0\end{pmatrix},\quad \mathcal{L}_1^1(\lambda)=\begin{pmatrix}c(\lambda) & 0\\ 0 & 1\end{pmatrix}.$$

In the case of the Heisenberg model $H_{XXX}=\sum_{j=1}^N h_{XXX}^{(j,j+1)}$ with

$$h_{XXX}=\tfrac{1}{2}[\sigma_x\otimes\sigma_x+\sigma_y\otimes\sigma_y+\sigma_z\otimes\sigma_z-\mathbb{1}],$$

functions $b(\lambda)$ and $c(\lambda)$ are

$$b(\lambda)=\frac{1}{1+\lambda},\quad c(\lambda)=\frac{\lambda}{1+\lambda}.$$

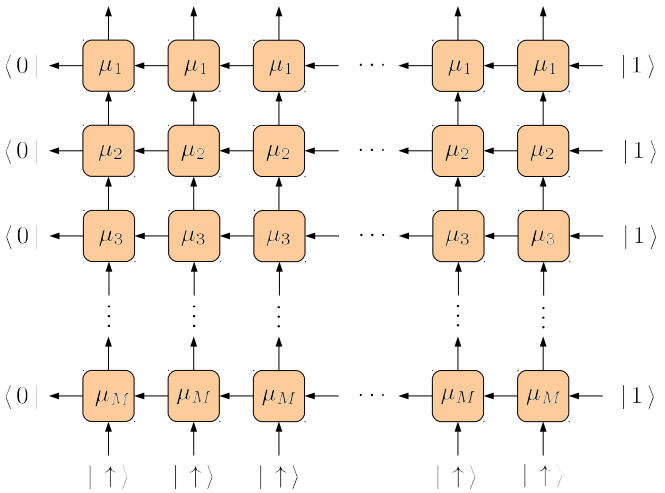

FIG. 2. (Color online) Tensor network constituting the Bethe eigenstate of the Heisenberg model or XXZ model with periodic boundary conditions.

For the XXZ model $H_{XXZ}(\Delta)=\sum_{j=1}^N h_{XXZ}^{(j,j+1)}(\Delta)$ with

$$h_{XXZ}(\Delta)=\tfrac{1}{2}[\sigma_x\otimes\sigma_x+\sigma_y\otimes\sigma_y+\Delta(\sigma_z\otimes\sigma_z-\mathbb{1})],$$

the functions read

$$b(\lambda)=\frac{\sinh(2i\eta)}{\sinh(\lambda+2i\eta)},\quad c(\lambda)=\frac{\sinh(\lambda)}{\sinh(\lambda+2i\eta)}.$$

The parameter η is related to the inhomogenity Δ in the XXZ model via $\Delta=\cos(2\eta)$.

Because of its "creation operator" property, there is an inherent structure in the MPO $B(\mu)$: each summand in the MPO $B(\mu)$ must be nonzero only if $k_1+\cdots+k_N=l_1+\cdots+l_N+1$. This global constraint can be reduced to the local constraint that the tensors $[\mathcal{L}_l^k(\mu)]_{r'}^r$ must be nonzero only if $r'=r+(k-l)$. This allows us to interpret the virtual indices as "creation-annihilation" counters: the right index r' is equal to the left index r if the physical state is unchanged, it is increased if a down-spin is created, and it is decreased if a down-spin is annihilated. Thus, the virtual indices transfer the information on how many down-spins are created and annihilated from left to right. Since the left boundary state is $\langle 0|$ and the right boundary state is $|1\rangle$, it is guaranteed that the whole MPO creates exactly one down-spin. With the restriction $r,r'\in\{0,1\}$ there are six possible configurations that fulfill the local constraint. In other words, only six entries of the tensor $[\mathcal{L}_l^k(\mu)]_{r'}^r$ are nonzero. These six nonzero entries are

$$[\mathcal{L}_0^0(\mu)]_0^0,\quad [\mathcal{L}_1^1(\mu)]_1^1,$$
$$[\mathcal{L}_1^0(\mu)]_0^1,\quad [\mathcal{L}_0^1(\mu)]_1^0,$$
$$[\mathcal{L}_0^0(\mu)]_1^1,\quad [\mathcal{L}_1^1(\mu)]_0^0,$$

which are consistent with the matrices written above.

The multiplication of all MPOs with the product state $|\mathrm{vac}\rangle$ evidently yields a MPS[6,8] with bond dimension 2^M. Since each MPO $B(\lambda)$ has the "creation operator" property to create one down-spin, the MPS contains exactly M down-spins. Explicitly, the MPS reads

$$|\Psi\rangle=\sum_{k_1\cdots k_N}\langle 0|\langle 0|\mathcal{A}^{k_1}\cdots\mathcal{A}^{k_N}|0\rangle|M\rangle|k_1,\ldots,k_N\rangle,$$

with matrices $\mathcal{A}^k$ being block diagonal in the sense that $\langle\alpha|\langle s|\mathcal{A}^k|\beta\rangle|s'\rangle\equiv[\mathcal{A}^k]_{\beta s'}^{\alpha s}$. α and β are the virtual indices, which range from 0 to $D-1$ (with D being the virtual dimension of the state). On the other hand, s and s' are the symmetry indices, which transfer the information about the number of down-spins from left to right. The local constraint that guarantees this information transfer is $s'=s+k$. This constraint determines the blocks $[\mathcal{A}^k]_{-s'}^{-s}$ that are nonzero and allows a sparse storage of the state. The left boundary state $\langle 0|$ and the right boundary state $|M\rangle$ fix the total number of down-spins of the MPS to M.

The MPS is constructed iteratively by applying the MPOs $B(\mu_1),\ldots,B(\mu_M)$ successively to the vacuum state $|\mathrm{vac}\rangle$. The state after m multiplications is evidently an MPS with m down-spins, which is denoted

$$|\Psi_m\rangle=\sum_{k_1\cdots k_N}\langle 0|\langle 0|\mathcal{A}_m^{k_1}\cdots\mathcal{A}_m^{k_N}|0\rangle|m\rangle|k_1,\ldots,k_N\rangle,$$

with $\mathcal{A}_m^k$ being block diagonal in the sense that $\langle\alpha|\langle s|\mathcal{A}_m^k|\beta\rangle|s'\rangle \equiv [\mathcal{A}_m^k]_{\beta s'}^{\alpha s}$ and fulfilling the constraint $s' = s + k$, as before. The application of the operator $B(\mu)$ to $|\Psi_m\rangle$ yields a state with $m+1$ down-spins:

$$|\Psi_{m+1}\rangle = \sum_{k_1\cdots k_N} \langle 0|\langle 0|\mathcal{A}_{m+1}^{k_1}\cdot\cdot\mathcal{A}_{m+1}^{k_N}|0\rangle|m+1\rangle|k_1,..,k_N\rangle. \tag{2}$$

The matrices $\mathcal{A}_{m+1}^k$ emerge from tensor products between $\mathcal{L}_l^k$ and $\mathcal{A}_m^l$, i.e., $\mathcal{A}_{m+1}^k = \sum_l \mathcal{L}_l^k \otimes \mathcal{A}_m^l$. In index notation,

$$\begin{aligned}&\langle\alpha|\langle r|\langle s|\mathcal{A}_{m+1}^k|\beta\rangle|r'\rangle|s'\rangle \\ &\quad = \sum_l \langle r|\mathcal{L}_l^k|r'\rangle\langle\alpha|\langle s|\mathcal{A}^l|\beta\rangle|s'\rangle.\end{aligned} \tag{3}$$

Because of the constraints $s' = s + l$ and $r' = r + (k - l)$, $S = s + r$ and $S' = s' + r'$ suggest themselves as new symmetry indices. With this definition, $S' = S + k$, as desired. S and S' range from 0 to $m+1$, since $s \in \{0,\ldots,m\}$ and $r \in \{0,1\}$. For $S = 0$ and $S = m+1$, there is the unique choice for $s = r = 0$ and $s = m, r = 1$, respectively. For $0 < S < m+1$, either $s = S$, $r = 0$, or $s = S-1$, $r = 1$. In this case, the index r must be kept to resolve this ambiguity. The index r can be incorporated into a new virtual index $\tilde{\alpha}$ as $\tilde{\alpha} = (\alpha, r)$. Thus, the dimension of the blocks doubles for $0 < S < m+1$. The column indices S', s', r', and β can be treated in the same way: for $S' = 0$ and $S' = m+1$, s' and r' are unambiguously defined; for $0 < S' < m+1$, there is an ambiguity that can be resolved by incorporating index r' into a new virtual index $\tilde{\beta} = (\beta, r')$. The matrices $\mathcal{A}_{m+1}^k$ in terms of the virtual indices $\tilde{\alpha}$ and $\tilde{\beta}$ and the symmetry indices S and S', i.e.,

$$\langle\tilde{\alpha}|\langle S|\mathcal{A}_{m+1}^k|\tilde{\beta}\rangle|S'\rangle := \langle\alpha|\langle r|\langle s|\mathcal{A}_{m+1}^k|\beta\rangle|r'\rangle|s'\rangle,$$

have the desired block form, which fulfills the constraint $S' = S + k$. Please refer to Table I for the dimensions of the block representations that arise for different values of m.

In the case of open boundary conditions, the Bethe ansatz has the same form as in (1), except that the creation operators are not single MPOs, but products of two MPOs:[25,26]

$$\mathcal{B}(\mu) = \sum_{s=0}^{1} \bar{B}_s(\mu) B_{1-s}(\mu).$$

$B_{1-s}(\mu)$ has the property to create $1-s$ down-spins, whereas $\bar{B}_s(\mu)$ creates s down-spins ($s \in \{0,1\}$), such that $\mathcal{B}(\mu)$ is a creation operator for exactly one down-spin, as before. In terms of the previously defined 2×2 matrices $\mathcal{L}_l^k(\mu)$, the MPOs read (see Appendix B)

$$B_s(\mu) = \sum_{\substack{k_1\cdots k_N \\ l_1\cdots l_N}} \langle s|\mathcal{L}_{l_1}^{k_1}(\mu)\cdots\mathcal{L}_{l_N}^{k_N}(\mu)|1\rangle o_{l_1}^{k_1}\otimes\cdots\otimes o_{l_N}^{k_N}$$

and

$$\bar{B}_{1-s}(\mu) = \sum_{\substack{k_1\cdots k_N \\ l_1\cdots l_N}} \langle s|\mathcal{L}_{l_1}^{k_1}(\mu)^T\cdots\mathcal{L}_{l_N}^{k_N}(\mu)^T|0\rangle o_{l_1}^{k_1}\otimes\cdots\otimes o_{l_N}^{k_N}.$$

The virtual indices of $B_s(\mu)$ indicate the balance of created versus annihilated down-spins from left to right. This is due to the local constraint on $[\mathcal{L}_l^k(\mu)]_{r'}^r$ that $r' = r + (k - l)$, as mentioned before. Since the left boundary vector is $\langle 0|$ and the right boundary vector is $|s\rangle$, the creation of s down-spins is guaranteed. In case of $\bar{B}_{1-s}(\mu)$, the MPO is built from the transposed matrices $\mathcal{L}_l^k(\mu)^T$, such that the local constraint on $[\mathcal{L}_l^k(\mu)^T]_{r'}^r$ is $r = r' + (k-1)$ and the virtual indices count the creation-annihilation balance from right to left. With the right boundary vector $|s\rangle$ and the left boundary vector $\langle 1|$, one down-spin is created for $s = 0$ and the number of down-spins is kept invariant for $s = 1$.

TABLE I. Disintegration of the matrices forming the MPS at step m, $|\Psi_m\rangle$, into blocks. The full size of the matrices is $D \times D$. The MPS has a conserved number of m down-spins.

m	D	
1	2	$2 = 1 \oplus 1$
2	4	$2 \otimes 2 = 1 \oplus 2 \oplus 1$
3	8	$2 \otimes 2 \otimes 2 = 1 \oplus 4 \oplus 2 \oplus 1$
4	16	$2 \otimes 2 \otimes 2 \otimes 2 = 1 \oplus 8 \oplus 4 \oplus 2 \oplus 1$
5	32	$2 \otimes 2 \otimes 2 \otimes 2 \otimes 2 = 1 \oplus 16 \oplus 8 \oplus 4 \oplus 2 \oplus 1$
6	64	$2 \otimes 2 \otimes 2 \otimes 2 \otimes 2 \otimes 2 = 1 \oplus 32 \oplus 16 \oplus 8 \oplus 4 \oplus 2 \oplus 1$

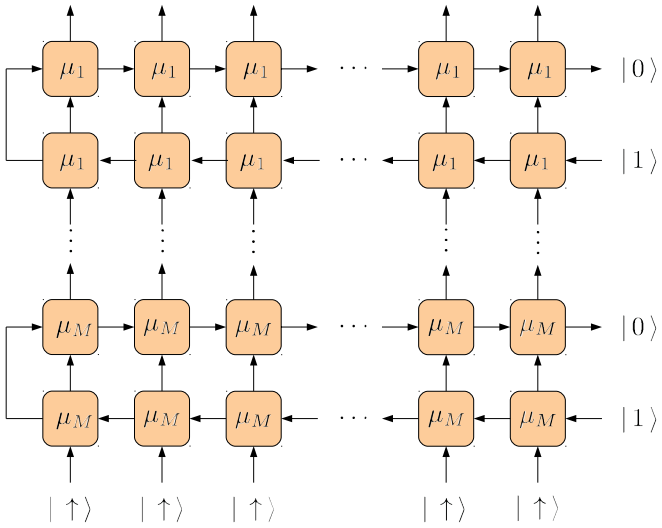

FIG. 3. (Color online) Tensor network constituting the Bethe eigenstate of the Heisenberg model or *XXZ* model with open boundary conditions.

The tensor-network representation for the Bethe state with open boundary conditions is shown in Fig. 3. It contains twice as many rows as the tensor network for periodic boundary conditions, which makes the contraction more challenging, in principle. However, as we see numerically, after a multiplication with an MPO pair $\mathcal{B}(\mu)$, the Schmidt rank of the state increases by a factor of only 2—not 4, as expected. This suggests that there should exist a representation with virtual dimension 2 also in the open boundary conditions case.

We explain in detail the algebraic Bethe ansatz for open and periodic boundary conditions in the picturesque tensor-network language in Appendixes A and B. These make evident that Bethe eigenstates have tensor-network representations as shown in Figs. 2 and 3.

III. MATRIX PRODUCT STATE APPROXIMATION TO BETHE SOLUTIONS

The calculation of expectation values with respect to a Bethe eigenstate of the form of (1) is a considerably complex problem, because it requires the contraction of the tensor network depicted in Fig. 1. This tensor network represents the correlation function $\langle\Psi(\mu_1,\ldots,\mu_M)|\sigma_x^{(i)}\sigma_x^{(j)}|\Psi(\mu_1,\ldots,\mu_M)\rangle$. It is composed of the network for $|\Psi(\mu_1,\ldots,\mu_M)\rangle$ shown in Fig. 2, the vertically mirrored network with conjugated tensor entries representing $\langle\Psi(\mu_1,\ldots,\mu_M)|$ and two operators $\sigma_x^{(i)}$ and $\sigma_x^{(j)}$ squeezed in between at sites i and j. A tensor network with such a structure also appears in connection with the calculation of partition functions of two-dimensional classical systems and one-dimensional quantum systems[23] and the calculation of expectation values with respect to PEPSs.[12–14] The complexity of contracting this network scales exponentially with the number of rows M or columns N (depending on the direction of contraction), which renders practical calculations infeasible.

To circumvent this problem, we attempt to perform the contraction in an approximative numerical way: the main idea is to consider the network in Fig. 2 as the time evolution of the state with all spins up by the evolution operators $B(\mu_1),\ldots,B(\mu_M)$ to the final state $|\Psi(\mu_1,\ldots,\mu_M)\rangle$. After each evolution step, the state remains an MPS, but the virtual dimension is increased by a factor of 2. Thus, we approximate the MPS after each evolution step by a simpler MPS with smaller virtual dimension. Of course, caution has to be used, because the operators $B(\mu_j)$ are not unitary and the intermediate states of the evolution can be nonphysical (i.e., they might have to be represented by an MPS with high virtual dimension). The Bethe network, however, bears an additional structure which can be taken advantage of: all evolution operators $B(\mu_j)$ commute, such that the operators $B(\mu_j)$ can be arbitrarily ordered. This allows us to choose the optimal ordering for the evolution with intermediate states that are least entangled. We discuss this in detail the following.

The algorithm consists of M steps $m=1,\ldots,M$: in the first step, the vacuum state $|\mathrm{vac}\rangle$ is multiplied by the MPO $B(\mu_1)$ to form the initial MPS $|\tilde{\Psi}_1\rangle$. In step $m>1$, the product $|\Psi_m\rangle \equiv B(\mu_m)|\tilde{\Psi}_{m-1}\rangle$ is approximated by the MPS $|\tilde{\Psi}_m\rangle$ that has maximal bond dimension $\tilde{D}$ and is closest to $|\Psi_m\rangle$. In other words, we try to solve the minimization problem

$$K := \||\Psi_m\rangle - |\tilde{\Psi}_m\rangle\|^2 \to \min \tag{4}$$

by optimizing over all matrices of the MPS $|\tilde{\Psi}_m\rangle$. This minimization problem also appears in the context of numerical calculation of expectation values with respect to PEPSs,[12–14] calculation of partition functions,[23] and (imaginary) time evolution of one-dimensional quantum systems.[8] We discuss it in detail in Appendix D. In this way, the MPS approximation of the Bethe state is obtained for $m=M$. Thereby, $\{\mu_1,\ldots,\mu_M\}$ are the solutions of the Bethe equations. The error of the approximation is well controlled in the sense that the expectation value of the energy can always be calculated with respect to the approximated MPS $|\tilde{\Psi}_M\rangle$ and compared to the exact energy available from the Bethe ansatz.

In order to make the algorithm more efficient, we take into account the "creation operator" property of the MPO $B(\mu)$: since each MPO $B(\mu)$ creates one down-spin, the MPS $|\Psi_m\rangle$ at step m contains exactly m down-spins. Explicitly, the MPS reads[27]

$$|\Psi_m\rangle = \sum_{k_1\cdots k_N} \langle 0|\langle 0|\mathcal{A}^{k_1}\cdots\mathcal{A}^{k_N}|0\rangle|m\rangle|k_1,\ldots,k_N\rangle,$$

with matrices $\mathcal{A}^k$ being block diagonal in the sense that $\langle\alpha|\langle s|\mathcal{A}^k|\beta\rangle|s'\rangle \equiv [\mathcal{A}^k]^{\alpha s}_{\beta s'}$. α and β are the virtual indices, which range from 0 to $D-1$ (with D being the virtual dimension of the state). On the other hand, s and s' are the symmetry indices, which transfer the information about the number of down-spins from left to right. The local constraint that guarantees this information transfer is $s'=s+k$. This constraint determines the blocks $[\mathcal{A}^k]^{-s}_{-s'}$ that are nonzero and allows a sparse storage of the state. The left boundary state $\langle 0|$ and the right boundary state $|m\rangle$ fix the total number of down-spins of the MPS to m. Optimization problem (4) at step m then consists in approximating the state $|\Psi_m\rangle$ with m down-spins by a state $|\tilde{\Psi}_m\rangle$ that also has m down-spins. This leads to a gain of a factor of m in time and memory.

Furthermore, there is a (mathematical) degree of freedom that can be used to improve the approximation. This degree of freedom is due to the commutativity property of $B(\mu)$: since $[B(\mu),B(\nu)]=0$ for all μ and ν, the ordering of the $B(\mu_j)'s$ in ansatz (1) is completely arbitrary. This is relevant insofar as the entanglement properties of the intermediate states $|\Psi_m\rangle$ $(1<m<M)$ are concerned. The intermediate states are *a priori* no physical ground states; i.e., there is no reason for them to lie in the set of MPS with low bond dimension. However, as we see numerically, there is always an ordering such that the intermediate states contain as little entanglement

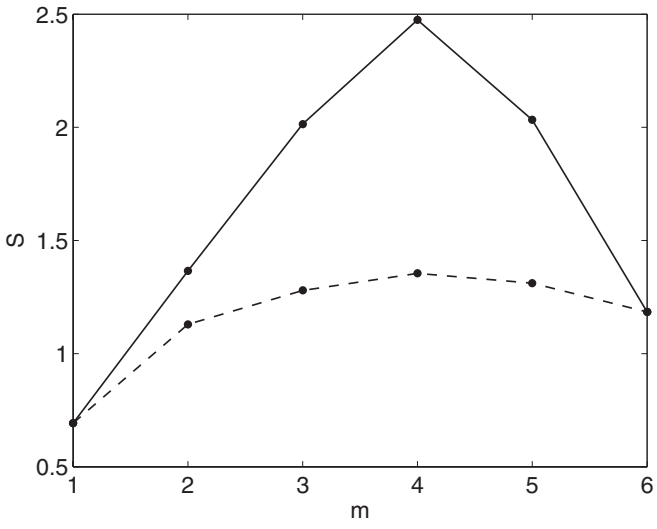

FIG. 4. Half-chain entropy as a function of the evolution step for the $N=12$ Heisenberg model with periodic boundary conditions. The rapidities $\mu_1,\ldots,\mu_6$ are obtained by solving the Bethe equations, (A15), with $z_j \leqslant z_{j+1}$ and relating μ_j and z_j via (A14). The lower (dashed) line is obtained with the orderings (435261), (435216), (432561), (432516), (345261), (345216), (342561), (342516) of the rapidities—corresponding to a symmetric filling of the Fermi set; the upper line is obtained with the orderings (531624), (426153), (351624), (246153).

as possible. This ordering we then use for calculating the approximation. That the ordering has a formidable effect can be gathered from Fig. 4 for the example of the ground state of the 12-site Heisenberg antiferromagnet with periodic boundary conditions. Here, the half-chain entropy of $|\Psi_m\rangle$ is plotted as a function of m for the best and the worst ordering. As shown, the entropy is highest in the intermediate steps and decreases at $m \to M$ when the state becomes a physical ground state.

IV. NUMERICAL RESULTS

Using the previously described method, we have obtained results for the Heisenberg model with periodic boundary conditions and the *XXZ* model with open boundary conditions. In the case of the Heisenberg model, we have investigated the two-spinon excited states with total spin $S = 1$ and total z spin $S_z = 1$. The energies of these states obtained by the Bethe ansatz as a function of the momentum for $N = 50$ spins are plotted in the right-hand inset in Fig. 5. With respect to these states, we have calculated the correlation functions $\langle \sigma_z^r \sigma_z^s \rangle$ and the corresponding structure factor:

$$S_z(q) = \frac{1}{N^2} \sum_{r,s} e^{iq(r-s)} \langle \sigma_z^r \sigma_z^s \rangle.$$

The structure factor $S_z(q)$ as a function of q for the three selected excited states (which are marked in the right-hand inset) can be gathered from Fig. 5. In order to judge the accuracy of the approximated Bethe MPS obtained with our method, we have compared the expectation values of the Hamiltonian with respect to these MPSs to the energies obtained from the Bethe ansatz. For the case $N = 50$, the relative error so obtained, plotted as a function of D for the selected excited states, can be gathered from the left-hand inset in Fig. 5. As shown, the error decreases with increasing D, but also with decreasing excitation energy. In Fig. 6, the structure factor at the point $q = \pi$, i.e., the squared staggered magnetization, is plotted as a function of the excitation energy and the momentum. Evidently, the excited states of the lowest branch show the highest staggered magnetization.

In Fig. 7 we plot the one-particle Green function $G(r) = \langle c_1^\dagger c_r \rangle \equiv \langle \sigma_1^+ \sigma_z^2 \cdots \sigma_z^{r-1} \sigma_r^- \rangle$ for the ground state of the $N = 50$ Heisenberg model and compare it to exact solutions for $G(2)$, $G(4)$, and $G(6)$ in the limit $N \to \infty$.[28] As shown, the deviation is only marginal and due to finite-size

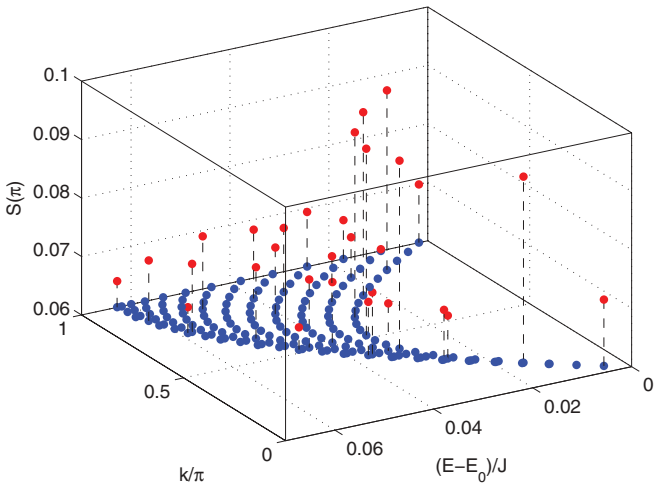

FIG. 6. (Color online) Structure factor $S(\pi)$ for selected two-spinon excited states of the $N = 50$ Heisenberg antiferromagnet as a function of the momentum and the excitation energy. The cutoff used is $D = 1000$.

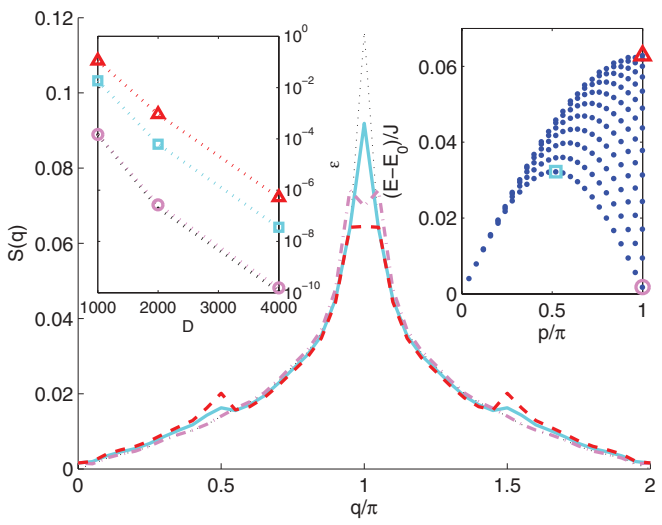

FIG. 5. (Color online) Structure factor for the ground state (dotted line) and three selected two-spinon excited states of the periodic $N = 50$ Heisenberg chain as a function of the wave vector q obtained from the approximated Bethe MPS with $D = 1000$. The three states are marked in the inset at the right, which shows all energies and momenta of the two-spinon excited states with total spin $S = 1$ and total z-spin $S_z = 1$. The insetat the left depicts the relative error in the energy as a function of D for the three selected two-spinon states.

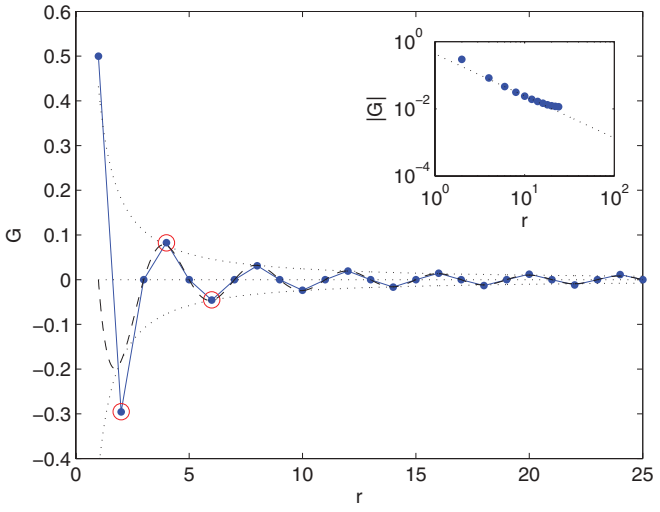

FIG. 7. (Color online) One-particle Green function $G(r) = \langle c_1^\dagger c_r \rangle$ for the ground state of the $N = 50$ Heisenberg antiferromagnet. Filled (blue) circles indicate results with respect to the approximated Bethe MPS with $D = 2000$. $G(2)$, $G(4)$, and $G(6)$ deviate only marginally from the exact results in the limit $N \to \infty$, indicated by the open (red) circles. The dotted (black) line shows the result $G(r) \propto \cos(k_F r) r^{-5/4}$ predicted by conformal field theory. Inset: Comparison of the enveloping function $r^{-5/4}$ with the absolute values of our results on a logarithmic scale, revealing a similar slope.

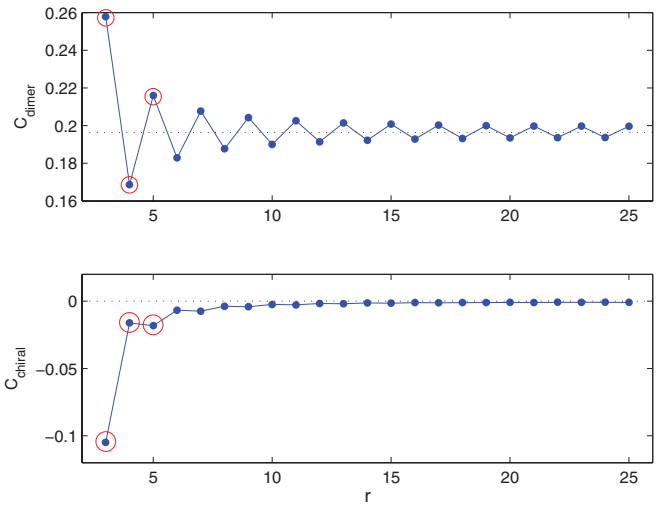

FIG. 8. (Color online) Dimer-dimer correlations (top) and chiral correlations (bottom) for the ground state of the $N = 50$ Heisenberg antiferromagnet, obtained with respect to the approximated Bethe MPS with $D = 2000$. Open (red) circles indicate the exact results obtained in the limit $N \to \infty$. The dotted (black) line indicates, in the upper plot, the square of the ground-state energy in the $N \to \infty$–limit, $e_0^2 = (\frac{1}{4} - \zeta_a(1))^2$, and, in the lower plot, the zero line.

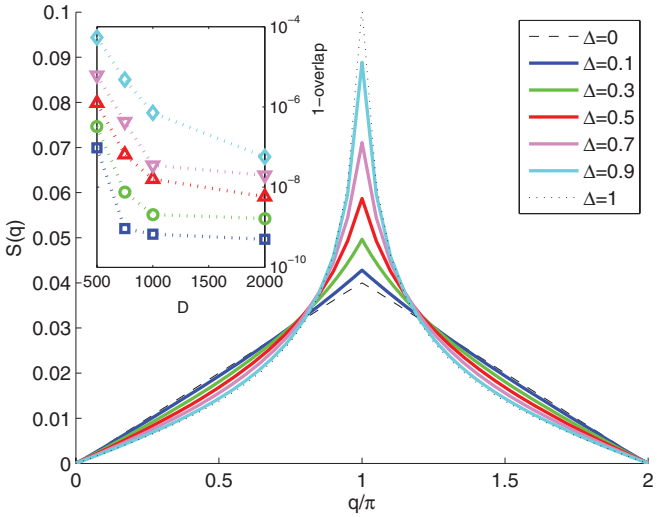

FIG. 9. (Color online) Structure factor $S(q)$ of the ground states of the $N = 50$ XXZ model with open boundary conditions for selected values of Δ obtained from the approximated Bethe MPS with $D = 1000$. The dashed (black) line marks the free fermion case $\Delta = 0$ and the dotted (black) line indicates the Heisenberg limit $\Delta = 1$. Inset: The overlap with MPS of virtual dimension $D = 400$ obtained from DMRG calculations.

corrections. The asymptotic behavior of the one-particle Green function is predicted by conformal field theory to be $G(r) \propto \cos(k_F r) r^{-5/4}$ with $k_F = \pi/2$.[28] This is strongly supported by our results, as can be gathered from Fig. 7 including the inset.

Other physically interesting correlation functions are the dimer-dimer correlation function

$$C_{\text{dimer}}(r) = \tfrac{1}{16}\langle(\vec{\sigma}_1 \cdot \vec{\sigma}_2)(\vec{\sigma}_r \cdot \vec{\sigma}_{r+1})\rangle$$

and the chiral correlation function

$$C_{\text{chiral}}(r) = \tfrac{1}{16}\langle(\vec{\sigma}_1 \times \vec{\sigma}_2) \cdot (\vec{\sigma}_r \times \vec{\sigma}_{r+1})\rangle,$$

which we plot in Fig. 8 for the Heisenberg model with 50 spins. The exact results for $r = 3,4,5$ in the limit $N \to \infty$ obtained in 28 deviate only marginally from our results. Also, as expected, the dimer-dimer correlations asymptotically tend to the square of the ground-state energy, i.e., to $e_0^2 = (\frac{1}{4} - \zeta_a(1))^2$, with $\zeta_a(s)$ denoting the alternating ζ function.

In the case of the XXZ model with open boundary conditions, we have studied the two-point correlations of the ground state. To get an impression of the quality of the obtained result, we computed the overlap with MPS states obtained from DMRG calculations. For the case of 50 spins, the overlap as a function of D can be gathered from the inset in Fig. 9 for different values of Δ. The structure factor $S(q)$ as a function of the wave vector q for different values of Δ evaluated with respect to the approximated Bethe MPS with $D = 1000$ is plotted in Fig. 9. The structure factor obtained for this D deviates only marginally from the structure factor obtained from the DMRG calculation.

V. CONCLUSIONS

Summing up, we have presented a method for approximative calculation of expectation values with respect to Bethe eigenstates. For this, we make use of the fact that a Bethe eigenstate is a product of MPOs applied to an MPS. We systematically reduce the virtual dimension after each multiplication and obtain an MPS with small virtual dimension that can be used for the calculation of any expectation value. We have shown the effective operation of this method by applying it to the Heisenberg antiferromagnet with periodic boundary conditions and the XXZ model with open boundary conditions. We have obtained results for the structure factor for excited states and compared our results for the ground state to DMRG calculations.

ACKNOWLEDGMENTS

V.M. and F.V. acknowledge support from the SFB projects FoQuS and ViCoM, the European project Quevadis, and the ERC grant Querg.

APPENDIX A: THE ALGEBRAIC BETHE ANSATZ

Even though there exist numerous excellent reviews about the algebraic Bethe ansatz,[2,29–32] we resketch here the ansatz in the picturesque tensor-network language for the sake of completeness. In this way, we can trace, how the tensor networks shown in Figs. 2 and 3 form exact eigenstates of integrable systems.

1. The Yang-Baxter algebra

In general, the starting point for the algebraic Bethe ansatz is the $R(\lambda,\mu)$ tensor,

$$R^{\alpha\beta}_{\alpha'\beta'}(\lambda,\mu), \tag{A1}$$

with α, β, α', and β' ranging from 1 to some "auxiliary" dimension d and λ, μ being some complex parameters. This tensor defines the model under study, as shown later.

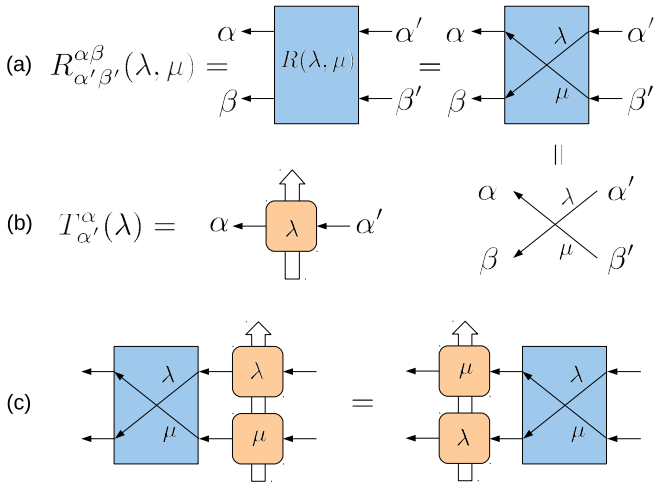

FIG. 10. (Color online) (a) Visualization of the four-index R tensor $R(\lambda,\mu)$. In the abbreviated version, it is visualized as two crossing arrows, with λ attached to the up-down arrow and μ attached to the down-up arrow. (b) Yang-Baxter algebra as a four-index tensor with two virtual indices (left-right) and two physical indices (up-down). (c) Defining equation for the Yang-Baxter algebra.

Graphically, the tensor is represented by two crossing arrows, as shown in Fig. 10(a), where λ and μ are associated with the up-down and down-up arrows, respectively. After joining indices $(\alpha\beta)$ and $(\alpha'\beta')$, tensor (A1) can also be interpreted as matrix $R(\lambda,\mu)$ acting on the vector space $V \otimes V$ (with $V = \mathbb{C}^d$).

The condition on the R tensor, (A1), is that it fulfills the Yang-Baxter equation (star-triangle relation). Writing

$$R^{(23)} = \mathbb{1} \otimes R,$$
$$R^{(12)} = R \otimes \mathbb{1},$$

the Yang-Baxter equation reads

$$R^{(23)}(\lambda,\mu)R^{(12)}(\lambda,\nu)R^{(23)}(\mu,\nu) = R^{(12)}(\mu,\nu)R^{(23)}(\lambda,\nu)R^{(12)}(\lambda,\mu).$$

The graphical representation of this equation is shown in Fig. 11. Another requirement is that solutions of the Yang-Baxter equation are regular, meaning that there exist a λ_0 and a ν_0, such that

$$R^{\alpha\beta}_{\alpha'\beta'}(\lambda_0,\nu_0) = \delta^{\alpha}_{\alpha'}\delta^{\beta}_{\beta'}. \tag{A2}$$

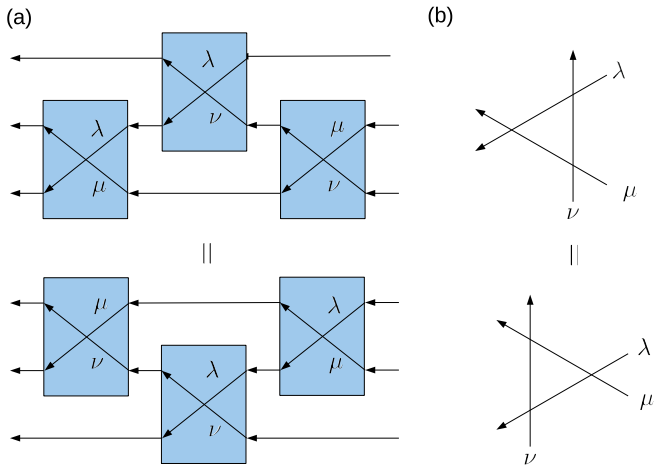

FIG. 11. (Color online) (a) Yang-Baxter equation in tensor-network form. (b) Abbreviated version.

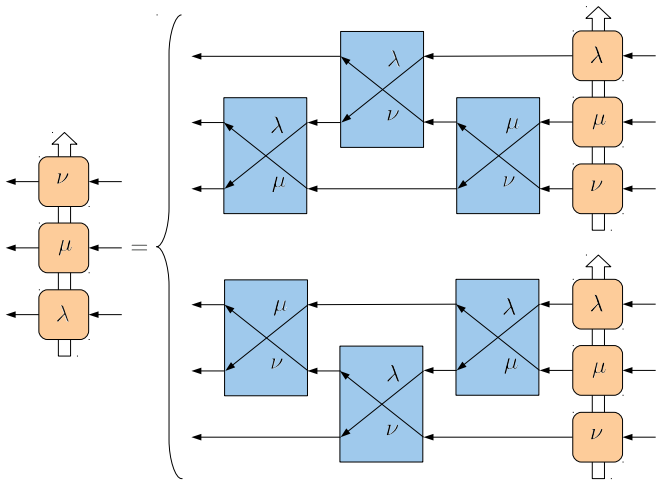

FIG. 12. (Color online) Inversion of the ordering of three composed Yang-Baxter algebras using R tensors. The inversion can be achieved in two ways, which requires that the R tensors fulfill the Yang-Baxter equation (Fig. 11).

The tensor $R(\lambda,\mu)$ defines the Yang-Baxter algebra $T^{\alpha}_{\alpha'}(\lambda)$ $(\alpha,\alpha' = 1,\ldots,d)$ by the relation

$$R^{\alpha\beta}_{\alpha'\beta'}(\lambda,\mu)T^{\alpha'}_{\alpha''}(\lambda)T^{\beta'}_{\beta''}(\mu) = T^{\alpha}_{\alpha'}(\mu)T^{\beta}_{\beta'}(\lambda)R^{\alpha'\beta'}_{\alpha''\beta''}(\lambda,\mu).$$

As usual, common indices are summed over. Defining the Monodromy $T(\lambda)$ as the matrix of operators

$$T(\lambda) = \begin{pmatrix} T^1_1(\lambda) & \cdots & T^1_d(\lambda) \\ \vdots & \ddots & \vdots \\ T^d_1(\lambda) & \cdots & T^d_d(\lambda) \end{pmatrix},$$

the definition of the Yang-Baxter algebra can be written as

$$R(\lambda,\mu)[T(\lambda)\tilde{\otimes}T(\mu)] = [T(\mu)\tilde{\otimes}T(\lambda)]R(\lambda,\mu), \tag{A3}$$

where the outer product "$\tilde{\otimes}$" acts in the space $V \otimes V$ in the sense that $[T(\mu)\tilde{\otimes}T(\lambda)]^{\alpha\beta}_{\alpha'\beta'} \equiv T^{\alpha}_{\alpha'}(\mu)T^{\beta}_{\beta'}(\lambda)$. $T(\lambda)$ can be considered as a four-index tensor: two "virtual" indices α and α' of dimension d select the operator $T^{\alpha}_{\alpha'}(\mu)$ within the matrix, and two "physical" indices operate as input and output index of the operator. $T(\lambda)$ is represented graphically in Fig. 10(b). The virtual indices are indicated as horizontal arrows; the physical input and output indices are indicated as vertical in- and outgoing double-arrows. Using this graphical notation, the definition of the Yang-Baxter algebra assumes the simple form shown in Fig. 10(c).

In this picture, $R(\lambda,\mu)$ has the property to permute the tensors $T(\lambda)$ and $T(\mu)$. There is, however, one ambiguity that arises: there are two ways to go from $T(\lambda)\tilde{\otimes}T(\mu)\tilde{\otimes}T(\nu)$ to $T(\nu)\tilde{\otimes}T(\mu)\tilde{\otimes}T(\lambda)$. This inversion of the ordering can be achieved either by exchanging, first, $\lambda \leftrightarrow \mu$, second, $\lambda \leftrightarrow \nu$, and, third, $\mu \leftrightarrow \nu$ or by exchanging, first, $\nu \leftrightarrow \mu$, second, $\lambda \leftrightarrow \nu$, and, third, $\lambda \leftrightarrow \mu$. This situation is depicted in Fig. 12.

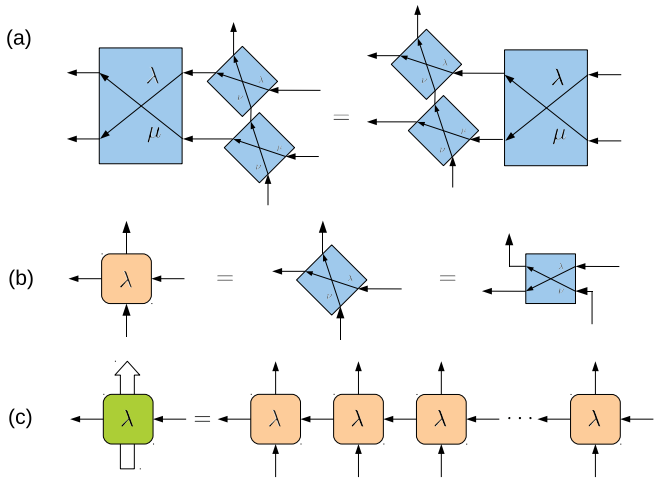

FIG. 13. (Color online) (a) Deformation of the Yang-Baxter equation, such that it yields the fundamental representation of the Yang-Baxter algebra. (b) Connection between the fundamental representation and the R tensor. (c) Formation of a more complex representation out of several fundamental representations.

Thus, both

$$R^{(12)}(\mu,\nu)R^{(23)}(\lambda,\nu)R^{(12)}(\lambda,\mu)[T(\lambda)\check{\otimes}T(\mu)\check{\otimes}T(\nu)] = [T(\lambda)\check{\otimes}T(\mu)\check{\otimes}T(\nu)]R^{(12)}(\mu,\nu)R^{(23)}(\lambda,\nu)R^{(12)}(\lambda,\mu)$$

and

$$R^{(23)}(\lambda,\mu)R^{(12)}(\lambda,\nu)R^{(23)}(\nu,\mu)[T(\lambda)\check{\otimes}T(\mu)\check{\otimes}T(\nu)] = [T(\lambda)\check{\otimes}T(\mu)\check{\otimes}T(\nu)]R^{(23)}(\lambda,\mu)R^{(12)}(\lambda,\nu)R^{(23)}(\nu,\mu)$$

must be fulfilled. These two equations, however, are compatible, because $R(\lambda,\mu)$ was required to fulfill the Yang-Baxter equation. This makes the definition of the algebra $T^{\alpha}_{\alpha'}(\lambda)$ consistent.

One representation of the Yang-Baxter algebra is easy to obtain—which is the fundamental representation. This representation is formed by the operators $L^{\alpha}_{\alpha'}(\lambda,\nu)$ acting on $\mathbb{C}^d$, defined as

$$\left[L^{\alpha}_{\alpha'}(\lambda,\nu)\right]^{k}_{l} = R^{k\alpha}_{\alpha' l}(\lambda,\nu). \tag{A4}$$

In the graphical picture, the operators correspond to a clockwise "rotation" of the R tensor by 45°, as shown in Fig. 13(b). The two indices attached to the horizontal arrow then become the virtual indices of the operator, and the vertical arrow carries the physical indices. That these operators are a valid representation is due to the fact that the defining equation

$$R(\lambda,\mu)[L(\lambda,\nu)\check{\otimes}L(\mu,\nu)] = [L(\mu,\nu)\check{\otimes}L(\lambda,\nu)]R(\lambda,\mu)$$

is just a "distortion" of the Yang-Baxter equation, as shown in Fig. 13(a). Up to now, the parameter ν in $L(\lambda,\nu)$ is arbitrary. Most conveniently, it is to set $\nu = \nu_0$.

Once one representation $L(\lambda)$ is known, more complex representations are obtained by concatenating the $L(\lambda)$'s horizontally, as depicted in Fig. 13(c). Here, operators $T^{\alpha}_{\alpha'}(\lambda)$ acting on $(\mathbb{C}^d)^{\otimes N}$ are constructed out of N simple operators $L^{\alpha}_{\alpha'}(\lambda)$ acting on $\mathbb{C}^d$ via

$$T^{\alpha}_{\alpha'}(\lambda) = \sum_{\alpha_2,\ldots,\alpha_N} L^{\alpha}_{\alpha_2}(\lambda)\otimes L^{\alpha_2}_{\alpha_3}(\lambda)\otimes\cdots\otimes L^{\alpha_N}_{\alpha'}(\lambda).$$

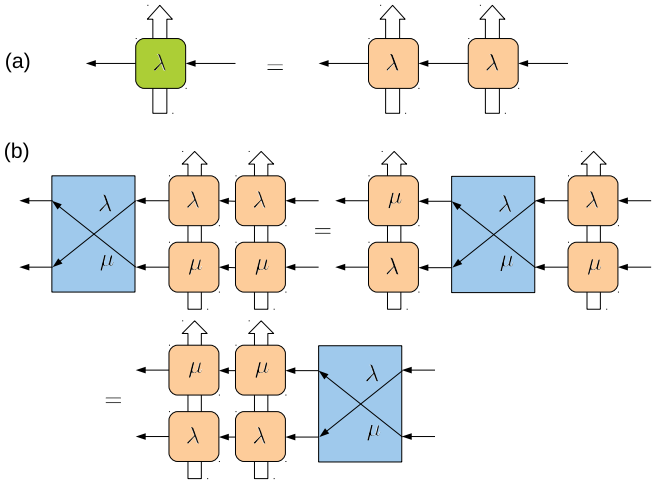

FIG. 14. (Color online) (a) Comultiplication property: formation of a new representation of the Yang-Baxter algebra out of two known representations. (b) Proof that the new representation still fulfills the defining equations for the Yang-Baxter algebra.

The outer product "$\otimes$" affects the physical indices. In index notation, the operators read

$$\left[T^{\alpha}_{\alpha'}(\lambda)\right]^{k_1\cdots k_N}_{l_1\cdots l_N} = \sum_{\alpha_2\cdots\alpha_N}\left[L^{\alpha}_{\alpha_2}(\lambda)\right]^{k_1}_{l_1}\left[L^{\alpha_2}_{\alpha_3}(\lambda)\right]^{k_2}_{l_2}\cdots\left[L^{\alpha_N}_{\alpha'}(\lambda)\right]^{k_N}_{l_N}.$$

The operators defined in such a way fulfill (A3), because the R tensor subsequently interchanges the operators $L^{\alpha}_{\alpha'}(\lambda)$ from left to right—as can be retraced from Fig. 14(b) for $N = 2$. Defining the matrices $\mathcal{L}^{k}_{l}(\lambda)$ as $\langle\alpha|\mathcal{L}^{k}_{l}(\lambda)|\alpha'\rangle := [L^{\alpha}_{\alpha'}(\lambda)]^{k}_{l}$, the operators $T^{\alpha}_{\alpha'}(\lambda)$ assume the form of MPOs,

$$T^{\alpha}_{\alpha'}(\lambda) = \sum_{\substack{k_1\cdots k_N\\ l_1\cdots l_N}}\langle\alpha|\mathcal{L}^{k_1}_{l_1}(\lambda)\cdots\mathcal{L}^{k_N}_{l_N}(\lambda)|\alpha'\rangle o^{k_1}_{l_1}\otimes\cdots\otimes o^{k_N}_{l_N},$$

with $o^{k}_{l} = |k\rangle\langle l|$.

The main building block of the algebraic Bethe ansatz is the transfer matrix $t(\lambda)$, obtained as the trace of the algebra $T^{\alpha}_{\alpha'}(\lambda)$,

$$t(\lambda) := \mathrm{tr}\,\{T(\lambda)\} \equiv \sum_{\alpha} T^{\alpha}_{\alpha}(\lambda).$$

The transfer matrix $t(\lambda)$ corresponds to $T^{\alpha}_{\alpha'}(\lambda)$ with contracted left and right indices α and α' [see Fig. 15(a)]. In the MPO picture, $t(\lambda)$ is represented by an MPO with periodic boundary conditions.[33] Due to Eq. (A3), which is fulfilled by the algebra, the transfer matrix has the property that $[t(\lambda),t(\mu)] = 0$ for all λ and μ. The way this property emerges from (A3) can immediately be read off from Fig. 15(b): first, starting out with the expression $t(\lambda)t(\mu)$, the identity in the form $\mathbb{1} = R(\lambda,\mu)^{-1}R(\lambda,\mu)$ can be inserted at the virtual bonds; second, $R(\lambda,\mu)$ can be used to exchange $T(\lambda)$ and $T(\mu)$; and, third, the cyclic property of the trace can be used to eliminate $R(\lambda,\mu)$ and $R(\lambda,\mu)^{-1}$ in order to end up with $t(\mu)t(\lambda)$.

This property makes $t(\lambda)$ the generator of an infinite set of commuting observables: if $t(\lambda)$ is Taylor expanded with respect to λ, $t(\lambda) = I_0 + \lambda I_1 + \lambda^2 I_2 + \ldots$, then $[I_j,I_k] = 0$ for all j and k. If one of the I_k values is equal to the Hamiltonian of a model, it is called *integrable*, since there

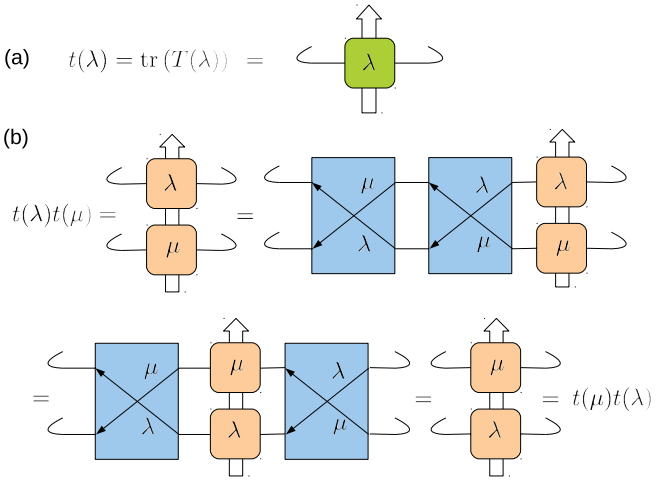

FIG. 15. (Color online) (a) Definition of the transfer matrix. (b) Proof that all transfer matrices commute.

exist infinitely many symmetries which commute mutually. In fact, any function of $t(\lambda)$ can be the generating function for a set of commuting observables, e.g., $\mathcal{F}(\lambda) = \log t(\lambda)$. The Taylor expansion of this function reads

$$\mathcal{F}(\lambda) = \mathcal{F}(\lambda_0) + (\lambda - \lambda_0)\mathcal{F}'(\lambda_0) + O((\lambda - \lambda_0)^2).$$

It turns out that $\mathcal{F}'(\lambda_0)$ is local in the sense that

$$\mathcal{F}'(\lambda_0) \equiv \frac{d}{d\lambda} \log t(\lambda)|_{\lambda=\lambda_0} = \sum_{i=1}^{N} h^{(i,i+1)},$$

with $h^{(i,i+1)}$ acting only on sites i and $i+1$. Thus, an integrable model is obtained, described by a local Hamiltonian,

$$H = \sum_{i=1}^{N} h^{(i,i+1)}. \tag{A5}$$

Thereby,

$$h^{k_1 k_2}_{l_1 l_2} = \frac{d}{d\lambda}\left[L^{k_1}_{l_2}(\lambda)\right]^{k_2}_{l_1}\Big|_{\lambda=\lambda_0} \tag{A6}$$

or

$$h = \frac{\partial}{\partial\lambda} R(\lambda, \nu_0)|_{\lambda=\lambda_0},$$

respectively. To see this connection, it has to be realized that, due to the regularity condition (A2), $t(\lambda_0)$ is equal to the cyclic shift operator, which shifts the whole lattice to the right by one site. The total momentum operator $\hat{P}$ is related to the cyclic shift operator according to

$$e^{i\hat{P}} = t(\lambda_0). \tag{A7}$$

Graphically, $t(\lambda_0)$ is built from $L^{\alpha}_{\alpha'}(\lambda_0)$ as shown in Fig. 16(a). The way the local Hamiltonian H emerges by differentiating the nonlocal expression $\mathcal{F}(\lambda)$ is sketched in Fig. 16(b). Since $\mathcal{F}'(\lambda_0) = t(\lambda_0)^{-1}t'(\lambda_0)$, the first row in the figure corresponds to the inverted cyclic shift operator $t(\lambda_0)^{-1}$ and the second row corresponds to the derivative $t'(\lambda_0)$. The derivative $t'(\lambda_0)$ disintegrates into a sum of N derivatives with respect to each of the tensors $L(\lambda)$ at sites $j = 1, \ldots, N$. As shown in the figure, term j has support at only two sites, j and $j+1$, and thus

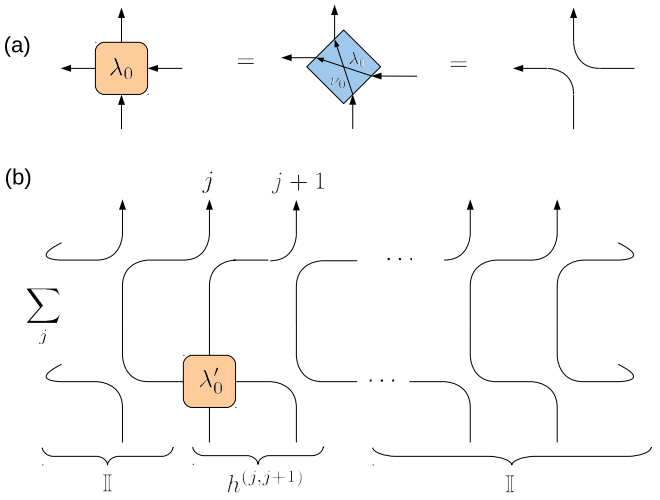

FIG. 16. (Color online) (a) Precondition on the R tensor: at some point $\lambda = \lambda_0$, the R tensor decomposes into the outer product of two identities. (b) Logarithmic derivative of the transfer matrix $t(\lambda)$ at the point $\lambda = \lambda_0$. The first row represents $t(\lambda_0)^{-1}$; the second row, $t'(\lambda_0)$.

corresponds to a two-site term that is related to the derivative $L'(\lambda_0)$ as formulated in (A6).

Models that emerge in such a way from combinations of fundamental representations are fundamental models. Examples are the spin-1/2 Heisenberg model and the XXZ model. In both cases, $d = 2$ and the R matrix assumes the form

$$R(\lambda,\mu) = \begin{pmatrix} 1 & & & \\ & b(\lambda,\mu) & c(\lambda,\mu) & \\ & c(\lambda,\mu) & b(\lambda,\mu) & \\ & & & 1 \end{pmatrix}. \tag{A8}$$

Also, $b(\lambda,\mu)$ and $c(\lambda,\mu)$ are of difference form, i.e., $b(\lambda,\mu) = b(\lambda-\mu)$ and $c(\lambda,\mu) = c(\lambda-\mu)$. This yields an R matrix of difference form as well: $R(\lambda,\mu) = R(\lambda-\mu)$. Explicitly, the functions b and c read

$$b(\lambda) = \frac{1}{1+\lambda},$$
$$c(\lambda) = \frac{\lambda}{1+\lambda}$$

for the Heisenberg model and

$$b(\lambda) = \frac{\sinh(2i\eta)}{\sinh(\lambda + 2i\eta)}, \tag{A9}$$

$$c(\lambda) = \frac{\sinh(\lambda)}{\sinh(\lambda + 2i\eta)} \tag{A10}$$

for the XXZ model. Evidently, in both cases, $R(0) = \mathbb{1}$, such that $\lambda_0 = 0$. In the case of the Heisenberg model, $R'(0) = h_{XXX}$ with

$$h_{XXX} = \tfrac{1}{2}[\sigma_x \otimes \sigma_x + \sigma_y \otimes \sigma_y + \sigma_z \otimes \sigma_z - \mathbb{1}\!\mathbb{1}].$$

In the XXZ case,

$$h_{XXZ}(\Delta) = \tfrac{1}{2}[\sigma_x \otimes \sigma_x + \sigma_y \otimes \sigma_y + \Delta(\sigma_z \otimes \sigma_z - \mathbb{1}\!\mathbb{1})]$$

is obtained via $R'(0) = 1/\sinh(2i\eta)h_{XXZ}(\Delta)$ with $\Delta = \cos(2\eta)$.

Models (fundamental and nonfundamental) with R matrix (A8) are $gl(2)$ generalized models. The Bethe ansatz for these models is especially simple and is described in the following.

2. Bethe ansatz for $gl(2)$ generalized models

The Yang-Baxter algebra with R matrix (A8) is generated by only four elements, such that the monodromy assumes the form

$$T(\lambda) = \begin{pmatrix} A(\lambda) & B(\lambda) \\ C(\lambda) & D(\lambda) \end{pmatrix}$$

with

$$A(\lambda) = T_0^0(\lambda), \quad C(\lambda) = T_0^1(\lambda),$$
$$B(\lambda) = T_1^0(\lambda), \quad D(\lambda) = T_1^1(\lambda).$$

The most important commutation relations of the algebra are

$$B(\lambda)B(\mu) = B(\mu)B(\lambda),$$
$$A(\lambda)B(\mu) = \frac{1}{c(\mu,\lambda)}B(\mu)A(\lambda) - \frac{b(\mu,\lambda)}{c(\mu,\lambda)}B(\lambda)A(\mu),$$
$$D(\lambda)B(\mu) = \frac{1}{c(\lambda,\mu)}B(\mu)D(\lambda) - \frac{b(\lambda,\mu)}{c(\lambda,\mu)}B(\lambda)D(\mu).$$

The precondition for the ansatz is that a representation must exist for which there is a pseudovacuum $|\mathrm{vac}\rangle$ that is an eigenstate of $A(\lambda)$ and $D(\lambda)$ and that is annihilated by $C(\lambda)$:

$$A(\lambda)|\mathrm{vac}\rangle = a(\lambda)|\mathrm{vac}\rangle,$$
$$D(\lambda)|\mathrm{vac}\rangle = d(\lambda)|\mathrm{vac}\rangle,$$
$$C(\lambda)|\mathrm{vac}\rangle = 0.$$

The goal is to diagonalize the transfer matrix $t(\lambda) = A(\lambda) + D(\lambda)$. Since all transfer matrices commute, $[t(\lambda),t(\mu)] = 0$, they have a common system of eigenvectors. Thus, all eigenvectors are independent of λ. The eigenvalue problem reads

$$t(\lambda)|\Psi\rangle = \tau(\lambda)|\Psi\rangle.$$

The Bethe ansatz

$$|\Psi(\mu_1,\ldots,\mu_M)\rangle = B(\mu_1)\cdots B(\mu_M)|\mathrm{vac}\rangle$$

fulfills the eigenvalue problem provided that the μ_k values fulfill the Bethe equations

$$\frac{d(\mu_n)}{a(\mu_n)} = \prod_{\substack{j=1 \\ j\neq n}}^{M} \frac{c(\mu_n,\mu_j)}{c(\mu_j,\mu_n)} \tag{A11}$$

$(n = 1,\ldots,M)$. The eigenvalue $\tau(\lambda)$ is then equal to

$$\tau(\lambda) = a(\lambda)\prod_{j=1}^{M}\frac{1}{c(\mu_j,\lambda)} + d(\lambda)\prod_{j=1}^{M}\frac{1}{c(\lambda,\mu_j)}.$$

The proof is obtained by utilizing algebraic relations only and can be gathered from Appendix C. From $\tau(\lambda)$, the eigenvalue of Hamiltonian (A5) is obtained as

$$E = \frac{\tau'(\lambda_0)}{\tau(\lambda_0)}. \tag{A12}$$

The total momentum is, according to (A7), equal to

$$p = -i\ln\tau(\lambda_0). \tag{A13}$$

3. Bethe ansatz for the Heisenberg model and the *XXZ* model

In the case of the Heisenberg model and *XXZ* model, this specializes as follows: the matrices $\mathcal{L}_l^k(\lambda)$ that build up the MPOs $T_{\alpha'}^{\alpha}(\lambda)$ have block form. Written out, they read

$$\mathcal{L}_0^0(\lambda) = \begin{pmatrix} 1 & 0 \\ 0 & c(\lambda) \end{pmatrix}, \qquad \mathcal{L}_1^0(\lambda) = \begin{pmatrix} 0 & 0 \\ b(\lambda) & 0 \end{pmatrix},$$

$$\mathcal{L}_0^1(\lambda) = \begin{pmatrix} 0 & b(\lambda) \\ 0 & 0 \end{pmatrix}, \qquad \mathcal{L}_1^1(\lambda) = \begin{pmatrix} c(\lambda) & 0 \\ 0 & 1 \end{pmatrix}.$$

These MPOs are symmetry conserving in the sense that $T_{\alpha'}^{\alpha}(\lambda)$ changes the number of down-spins by $\alpha' - \alpha$. This is due to the local constraint that $[\mathcal{L}_l^k(\lambda)]_{\alpha'}^{\alpha}$ are nonzero only if $\alpha' = \alpha + (k - l)$, as discussed in Sec. II.

Using these considerations, the vacuum state is obviously the state with no down-spins, namely,

$$|\mathrm{vac}\rangle = |0\rangle \otimes \cdots \otimes |0\rangle$$

$(0 \equiv\uparrow,\ 1 \equiv\downarrow)$. This state is annihilated by $C(\lambda)$ and is an eigenvector of $A(\lambda)$ and $D(\lambda)$ with eigenvalues

$$a(\lambda) = 1, \quad d(\lambda) = c(\lambda)^N.$$

The Bethe ansatz state

$$|\Psi(\mu_1,\ldots,\mu_M)\rangle = B(\mu_1)\cdots B(\mu_M)|\mathrm{vac}\rangle$$

is a state with M down-spins, i.e., with magnetization in the z direction equal to $S_z = \frac{1}{2}N - M$.

The Bethe equations obtained by the algebraic Bethe ansatz are equal to the equations obtained by the coordinate Bethe ansatz. In the case of the Heisenberg model, it is advantageous to introduce variables z_j that are related to μ_j in (A11) via

$$\mu_j = \frac{z_j}{2i} - \frac{1}{2} \tag{A14}$$

for a direct comparison with results of the coordinate Bethe ansatz:[1,34–37] in terms of these variables, the Bethe equations read

$$\left(\frac{z_n - i}{z_n + i}\right)^N = \prod_{\substack{j=1 \\ j\neq n}}^{M} \frac{z_n - z_j - 2i}{z_n - z_j + 2i} \tag{A15}$$

with $n = 1,\ldots,M$. From the Bethe solutions $\{z_j\}$, the energy is obtained using (A12) as

$$E = \frac{\tau'(0)}{\tau(0)} = -\sum_{j=1}^{M}\frac{4}{z_j^2 + 1}.$$

According to (A13), the total momentum $\hat{P}$ has eigenvalue

$$p = -i\ln\tau(0) = \sum_{j=1}^{M}\left(-i\ln\frac{z_j + i}{z_j - i}\right).$$

The addends are usually referred to as magnon momenta, which can be written as

$$p_j = \pi - 2\arctan(z_j)$$

using the identity

$$\arctan(z) = \frac{1}{2i} \ln \frac{1+iz}{1-iz}.$$

In terms of the magnon momenta p_j, the total momentum reads

$$p = \sum_{j=1}^{M} p_j \tag{A16}$$

and the energy is equal to

$$E = -2 \sum_{j=1}^{M} (1 - \cos(p_j)).$$

To solve the Bethe equations, (A15), it is advantageous to bring them to their logarithmic form

$$N p_n = 2\pi I_n + \sum_{\substack{j=1 \\ j \neq n}}^{M} \Theta(p_n, p_j),$$

where

$$2 \cot \frac{\Theta(p,q)}{2} = \cot \frac{p}{2} - \cot \frac{q}{2}$$

and I_j are integers $\in \{0, \ldots, N\}$. Solutions can then be found iteratively, as described in 36. The ground-state configuration for N even and $M = N/2$ is $(I_1, \ldots, I_M) = (1, 3, \ldots, N-1)$.

In the case of the XXZ model, it is advantageous to introduce the variables z_j related to μ_j in (A11) via

$$\mu_j = z_j - i\eta + i\frac{\pi}{2}$$

to compare with the coordinate Bethe ansatz.[38,39] The Bethe equations then read

$$\left(\frac{\cosh(z_n - i\eta)}{\cosh(z_n + i\eta)} \right)^N = \prod_{\substack{j=1 \\ j \neq n}}^{M} \frac{\sinh(z_n - z_j - 2i\eta)}{\sinh(z_n - z_j + 2i\eta)}.$$

From the Bethe solutions $\{z_j\}$, the energy is obtained as

$$E = \sinh(2i\eta) \frac{\tau'(0)}{\tau(0)} = 2 \sum_{j=1}^{M} \frac{\sin(2\eta)^2}{\cos(2\eta) + \cosh(2z_j)}.$$

The total momentum obtained from (A13) is again of the form (A16) with

$$p_j = -2 \arctan\left(\tanh(z_j) \tan(\eta) \right).$$

In terms of the momenta p_j, the energy can be expressed as

$$E = -2 \sum_{j=1}^{M} (\Delta - \cos(p_j)).$$

The Bethe equations in their logarithmic form read

$$N p_n = 2\pi I_n + \sum_{\substack{j=1 \\ j \neq n}}^{M} \Theta(p_n, p_j),$$

with

$$\cot \frac{\Theta(p,q)}{2} = \frac{\Delta \sin \frac{p-q}{2}}{\cos \frac{p+q}{2} - \Delta \cos \frac{p-q}{2}} \tag{A17}$$

and $I_j \in \{0, \ldots, N\}$. The ground-state configuration for N even and $M = N/2$ is again found with $(I_1, \ldots, I_M) = (1, 3, \ldots, N-1)$.

APPENDIX B: ALGEBRAIC BETHE ANSATZ FOR OPEN BOUNDARY CONDITIONS

The method described for periodic boundary conditions is generalizeable to models with open boundary conditions and boundary fields.[25,26,40] We resketch here the ansatz for open boundary conditions following Sklyanin[26] closely, using a picturesque language.

For the following it is required that the R tensor fulfills several conditions. To express these, it is convenient to define the permutation operator

$$P = \sum_{i,j} |j,i\rangle\langle i,j|,$$

which permutes two indices. Using the matrix notation $R(\lambda, \mu)$ from Appendix A, i.e., considering the R tensor as a matrix acting on $V \otimes V$ with $V = \mathbb{C}^d$, a variant of the R tensor with the first two indices permuted can be defined as

$$\mathcal{R}(\lambda, \mu) = P R(\lambda, \mu).$$

The basic assumption is that the R tensor fulfills the symmetry condition

$$P R(\lambda, \mu) P = R(\lambda, \mu)$$

[see Fig. 17(a)]. Then the R tensor can be expressed by just two crossing arrows and it is not necessary to distinguish between them by marking them with the arguments. In fact, it is assumed in the following that R is of difference form, i.e., $R(\lambda, \mu) = R(\lambda - \mu)$. Thus, the tensor $R(\lambda - \mu)$ is characterized by two crossing arrows together with the argument $\lambda - \mu$, as shown by the rightmost depiction in

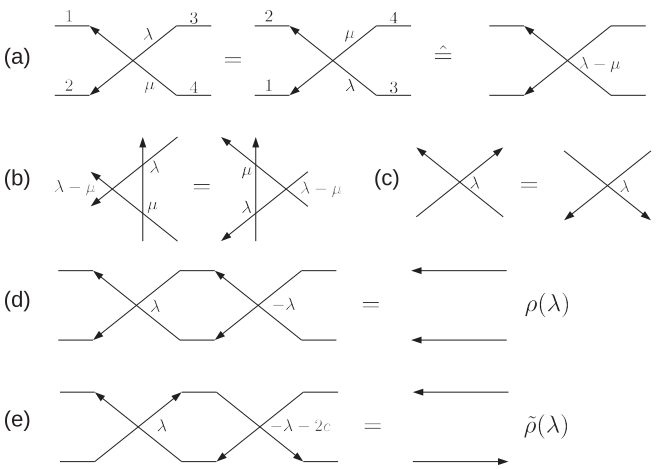

FIG. 17. (a) Permutation symmetry. (b) Yang-Baxter equation. (c) Partial transposition symmetry. (d) Unitary condition. (e) Crossing unitary condition.

Fig. 17(a). Using this notation, the Yang-Baxter equation assumes the form shown in Fig. 17(b).

It is, furthermore, useful to define the partial transposition

$$[\mathcal{R}(\lambda)^{t_1}]^{\alpha\beta}_{\alpha'\beta'} = [\mathcal{R}(\lambda)]^{\alpha'\beta}_{\alpha\beta'},$$

which is equivalent to flipping the direction of the "up-down" arrow. In analogy,

$$[\mathcal{R}(\lambda)^{t_2}]^{\alpha\beta}_{\alpha'\beta'} = [\mathcal{R}(\lambda)]^{\alpha\beta'}_{\alpha'\beta}$$

corresponds to flipping the direction of the "down-up" arrow. Accordingly, the partial transposition symmetry condition

$$\mathcal{R}(\lambda)^{t_1} = \mathcal{R}(\lambda)^{t_2}$$

is expressed by Fig. 17(c).

Further conditions are the unitarity condition

$$\mathcal{R}(\lambda)\mathcal{R}(-\lambda) = \rho(\lambda) \tag{B1}$$

and the crossing unitarity condition

$$\mathcal{R}(\lambda)^{t_1}\mathcal{R}(-\lambda - 2c)^{t_1} = \tilde{\rho}(\lambda), \tag{B2}$$

with $\rho(\lambda)$ and $\tilde{\rho}(\lambda)$ being some scalar functions of λ and c denoting a constant characterizing the R tensor. These conditions are represented by Figs. 17(d) and 17(e).

1. Reflection algebras

As the Bethe ansatz for periodic boundary conditions is based on the Yang-Baxter algebra, the footing of the open boundary conditions ansatz are the reflection algebras $\mathcal{K}^-(\lambda)$ and $\mathcal{K}^+(\lambda)$ spanned by $\{\mathcal{K}^-_{\alpha\beta}(\lambda)|\alpha,\beta = 1,\ldots,d\}$ and $\{\mathcal{K}^+(\lambda)_{\alpha\beta}|\alpha,\beta = 1,\ldots,d\}$. The graphical representation of these two algebras is shown in Fig. 18(a): as in the case of the Yang-Baxter algebra, each of the two algebras is considered as a four-index tensor with two "virtual" indices α and β of dimension d, represented by the horizontal arrows, and two "physical" indices (corresponding to the input and output

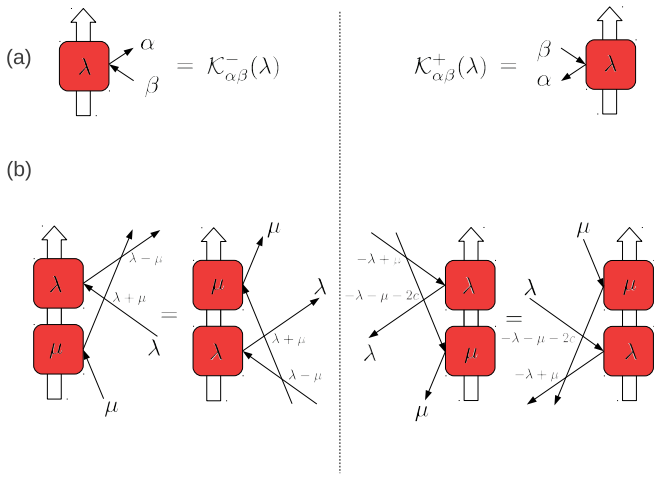

FIG. 18. (Color online) (a) Graphical representation of the reflection algebras $\mathcal{K}^-(\lambda)$ and $\mathcal{K}^+(\lambda)$. Horizontal arrows indicate the virtual indices α and β; the vertical arrow indicates physical indices, i.e., the input and output indices of the operators $\mathcal{K}^-_{\alpha\beta}(\lambda)$ and $\mathcal{K}^+_{\alpha\beta}(\lambda)$, respectively. (b) Defining equations for the reflection algebras (reflection equations). Each intersection of two lines represents an R tensor. The argument of the R tensor is written next to the intersection.

indices of the operators $\mathcal{K}^-_{\alpha\beta}(\lambda)$ and $[\mathcal{K}^+_{\alpha\beta}(\lambda)]$ respectively), represented by the vertical arrows. The only difference from the Yang-Baxter case is that the virtual indices are both on the right-hand side of the tensor in the case of $\mathcal{K}^-(\lambda)$ and on the left-hand side in the case of $\mathcal{K}^+(\lambda)$. The correspondence to the monodromy in the open boundary condition case is the matrix of operators

$$\mathcal{K}^{\pm}(\lambda) = \begin{pmatrix} \mathcal{K}^{\pm}_{11}(\lambda) & \cdots & \mathcal{K}^{\pm}_{1d}(\lambda) \\ \vdots & \ddots & \vdots \\ \mathcal{K}^{\pm}_{d1}(\lambda) & \cdots & \mathcal{K}^{\pm}_{dd}(\lambda) \end{pmatrix}.$$

The defining equations for the reflection algebras are the reflection equations, represented by the tensor network in Fig. 18(b). In that figure, each intersection of two lines represents an R tensor. The argument of the R tensor is written next to the intersection. Algebraically, the reflection equations read

$$\begin{aligned}&\mathcal{R}(\lambda-\mu)\overset{1}{\mathcal{K}}{}^-(\lambda)\mathcal{R}(\lambda+\mu)\overset{2}{\mathcal{K}}{}^-(\mu)\\ &\quad= \overset{2}{\mathcal{K}}{}^-(\mu)\mathcal{R}(\lambda+\mu)\overset{1}{\mathcal{K}}{}^-(\lambda)\mathcal{R}(\lambda-\mu)\end{aligned}$$

and

$$\begin{aligned}&\mathcal{R}(-\lambda+\mu)[\overset{1}{\mathcal{K}}{}^+(\lambda)]^{t_1}\mathcal{R}(-\lambda-\mu-2c)[\overset{2}{\mathcal{K}}{}^+(\mu)]^{t_2}\\ &\quad= [\overset{2}{\mathcal{K}}{}^+(\mu)]^{t_2}\mathcal{R}(-\lambda-\mu-2c)[\overset{1}{\mathcal{K}}{}^+(\lambda)]^{t_1}\mathcal{R}(-\lambda+\mu),\end{aligned}$$

with

$$\begin{aligned}\overset{1}{\mathcal{K}}{}^{\pm}(\lambda) &= \mathcal{K}^{\pm}(\lambda)\check{\otimes}\mathbb{1},\\ \overset{2}{\mathcal{K}}{}^{\pm}(\lambda) &= \mathbb{1}\check{\otimes}\mathcal{K}^{\pm}(\lambda).\end{aligned}$$

The outer product "$\check{\otimes}$" is thereby interpreted as in (A3), and $\mathbb{1}$ is the $d \times d$ identity matrix.

Using these algebras, it is possible to define a commuting set of transfer matrices via

$$\tau(\lambda) = \mathrm{tr}(\mathcal{K}^-(\lambda)\mathcal{K}^+(\lambda)).$$

Graphically, $\tau(\lambda)$ corresponds to $\mathcal{K}^-(\lambda)$ and $\mathcal{K}^+(\lambda)$ being glued together, as shown in Fig. 19(a). The commutativity of the transfer matrices, $[\tau(\lambda),\tau(\mu)] = 0$, can be proven using the unitary and crossing unitary conditions (B1) and (B2) and the reflection equations. The proof is sketched in Fig. 19(b): starting out with $\tau(\lambda)\tau(\mu)$, the line connecting $\mathcal{K}^+(\mu)$ and $\mathcal{K}^-(\mu)$ can be pulled over the line lying above, which connects $\mathcal{K}^-(\lambda)$ and $\mathcal{K}^+(\lambda)$, using (B2) and over the topmost arrow connecting the two λ algebras using (B1). Next, the network is mirrored vertically by using the reflection equations. Finally, the drawn-out line is pushed back using (B1) and (B2), which leads to $\tau(\mu)\tau(\lambda)$, as desired.

What remains is to find concrete representations of the reflection algebras. Examples of simple representations with physical dimension 1 have already been found.[25] More complex representations can be constructed by assembling a known representation with two R tensors in the way shown in Fig. 20(a). The physical dimension of the new representation is thereby increased by a factor d. That this assembly is indeed a valid representation can be proven using the Yang-Baxter equation and the reflection equations. The proof is sketched in Fig. 21.

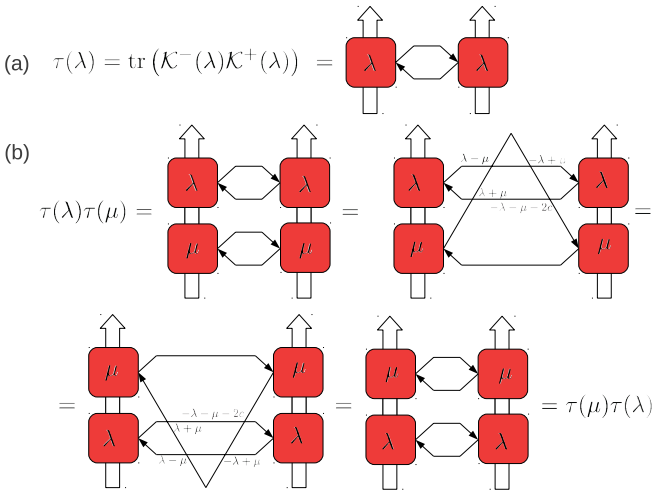

FIG. 19. (Color online) (a) Definition of the transfer matrix. (b) Proof of the commuting property of the transfer matrix, $[\tau(\lambda), \tau(\mu)] = 0$.

Thus, starting out with a simple representation with physical dimension 1 for $\mathcal{K}^-(\lambda)$, a representation with physical dimension d^N is obtained after N iterations with the relation expressed in Fig. 20(a). The structure of the representation after N iterations can be gathered from Fig. 20(b). Assuming a simple representation with physical dimension 1 for $\mathcal{K}^+(\lambda)$ [depicted in Fig. 20(c)], the transfer matrix assumes the form shown in Fig. 20(d).

For the sake of simplicity, we choose the simple representations with physical dimension 1 equal to the identity (which is a valid representation that fulfills the reflection equations). Using the notation for the fundamental representation of the Yang-Baxter algebra introduced in Eq. (A4) and Fig. 13(b), the representations of the algebras $\mathcal{K}^-(\lambda)$ and $\mathcal{K}^+(\lambda)$ look as

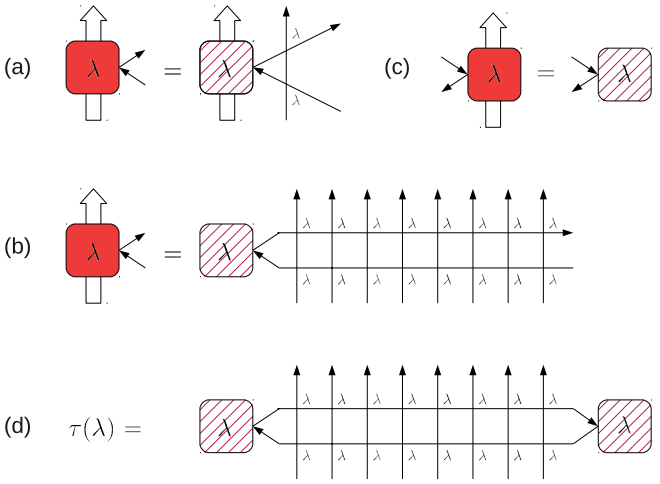

FIG. 20. (Color online) (a) Composition of a new representation of $\mathcal{K}^-(\lambda)$ out of one pair of R tensors and a known representation of $\mathcal{K}^-(\lambda)$ (that already fulfills the reflection equations). The known representation is indicated by the shaded area. (b) Simple representation of $\mathcal{K}^+(\lambda)$ with physical dimension 1. (c) Composition of a complex representation of $\mathcal{K}^-(\lambda)$ of dimension d^N by attaching N pairs of R tensors to a simple representation with physical dimension 1. (d) Transfer matrix built from representations (b) and (c).

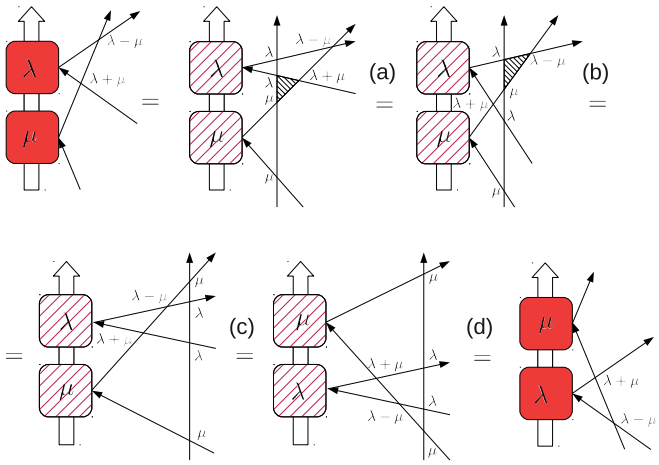

FIG. 21. (Color online) Proof that the composed representation shown in Fig. 20(a) fulfills the reflection equations: the main idea of the first two steps, (a, b), is to pull the vertical line rightmost by applying the Yang-Baxter equation twice. The three R tensors to which the Yang-Baxter equation is applied are shown as the shaded triangles. The new situation now allows the application of the reflection equations, as shown in step (c). The last step (d) consists in pushing the vertical line back by applying the Yang-Baxter equation twice, such as in steps (a) and (b), but in reverse order.

shown in Fig. 22(a). The transfer matrix assumes the form depicted in Fig. 22(b). Algebraically, the representation of $\mathcal{K}^-(\lambda)$ is then the product of two MPOs:

$$\mathcal{K}^-_{\alpha\beta}(\lambda) = \sum_{s=1}^{d} \bar{K}^-_{s\alpha}(\lambda) K^-_{s\beta}(\lambda). \tag{B3}$$

In terms of the previously defined matrices $\mathcal{L}^k_l(\lambda)$, the MPOs read

$$K^-_{s\beta}(\lambda) = \sum_{\substack{k_1 \cdots k_N \\ l_1 \cdots l_N}} \langle s|\mathcal{L}^{k_1}_{l_1}(\lambda) \cdots \mathcal{L}^{k_N}_{l_N}(\lambda)|\beta\rangle o^{k_1}_{l_1} \otimes \cdots \otimes o^{k_N}_{l_N}$$

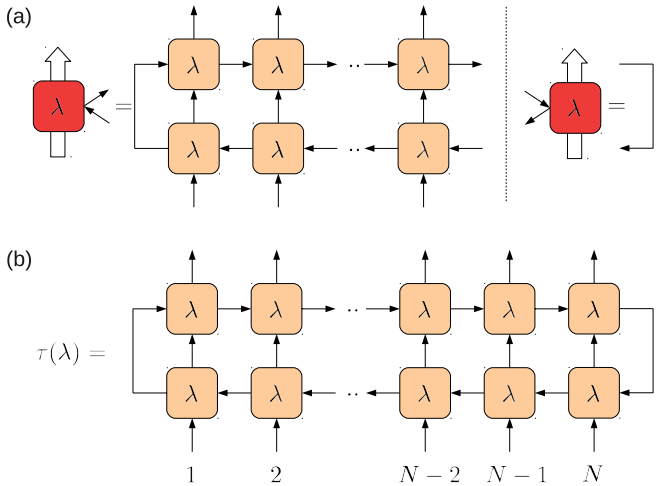

FIG. 22. (Color online) (a) Representation of $\mathcal{K}^-(\lambda)$ and $\mathcal{K}^+(\lambda)$ for open boundary conditions. (b) Transfer matrix built from these representations.

and

$$\bar{K}^{-}_{s\alpha}(\lambda) = \sum_{\substack{k_1\cdots k_N \\ l_1\cdots l_N}} \langle s|\mathcal{L}^{k_1}_{l_1}(\lambda)^T \cdots \mathcal{L}^{k_N}_{l_N}(\lambda)^T|\alpha\rangle o^{k_1}_{l_1} \otimes \cdots \otimes o^{k_N}_{l_N},$$

with $o^k_l = |k\rangle\langle l|$. The representation of $\mathcal{K}^+(\lambda)$ has physical dimension 1 and is equal to the identity with respect to the virtual indices, i.e.,

$$\mathcal{K}^+_{\alpha\beta}(\lambda) = \delta_{\alpha\beta}.$$

The transfer matrix constructed in this way is indeed related to a local Hamiltonian with open boundary conditions. This Hamiltonian is obtained as the derivative of the transfer matrix at the point λ_0 at which the R tensor is equal to the identity [see (A2)]. Explicitly, the obtained Hamiltonian is of the form

$$H \equiv \sum_{i=1}^{N-1} h^{(i,i+1)} + \frac{1}{d}\mathrm{tr}_a h^{(N,a)} \tag{B4}$$

and related to the transfer matrix via

$$H = \frac{1}{2d}\tau'(\lambda_0).$$

In (B4), the symbol a refers to an auxiliary system that is traced out. Using the notation from Appendix A, this relation is seen as follows: the derivative $\tau'(\lambda_0)$ disintegrates into a sum of $2N$ terms, each term containing one tensor differentiated at λ_0 and $2N-1$ tensors evaluated at λ_0. Due to the regularity condition (A2) of the R tensor, the tensors evaluated at λ_0 assume the simple form shown in Fig. 16(a). As can be gathered from Figs. 23 and 24, each differentiated tensor at site i corresponds to a two-site term $h^{(i,i+1)}$ for $i = 1,\ldots,N-1$ [with h being defined in (A6)]. For $i = N$, two indices of the tensor are traced out, which leads to the one-site term, $\mathrm{tr}_a h^{(N,a)}$.

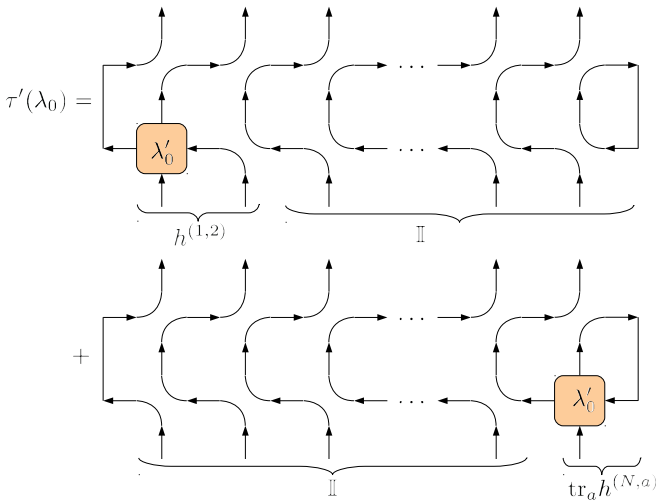

FIG. 23. (Color online) Derivation of the open boundary condition Hamiltonian by a derivative of the transfer matrix shown in Fig. 22(b) at point λ_0. Part I.

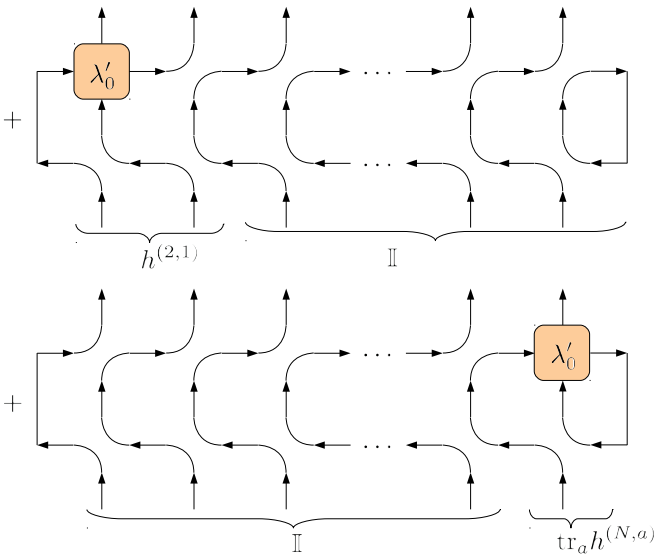

FIG. 24. (Color online) Derivation of the open boundary condition Hamiltonian by a derivative of the transfer matrix shown in Fig. 22(b) at point λ_0. Part II.

2. Bethe ansatz for the *XXZ* model with open boundary conditions

For the *XXZ* model, the virtual dimension d is equal to 2, such that the monodromy can be written in the form

$$\mathcal{K}^-(\lambda) = \begin{pmatrix} \mathcal{A}(\lambda) & \mathcal{B}(\lambda) \\ \mathcal{C}(\lambda) & \mathcal{D}(\lambda) \end{pmatrix},$$

with

$$\mathcal{A}(\lambda) = \mathcal{K}^-_{00}(\lambda), \quad \mathcal{C}(\lambda) = \mathcal{K}^-_{10}(\lambda),$$
$$\mathcal{B}(\lambda) = \mathcal{K}^-_{01}(\lambda), \quad \mathcal{D}(\lambda) = \mathcal{K}^-_{11}(\lambda).$$

The R tensor has the form of (A8), with $b(\lambda)$ and $c(\lambda)$ being defined by (A9) and (A10). It fulfills the regularity condition (A2) at the point $\lambda_0 = 0$, the unitarity condition (B1) with $\rho(\lambda) = 1$, and the crossing unitarity condition (B2) with $c = 2i\eta$ and $\tilde{\rho}(\lambda) = 1 - \sin(2\eta)^2/\sin(2\eta - i\lambda)^2$. Using representation (B3) for $\mathcal{K}^-(\lambda)$, the R tensor generates the Hamiltonian

$$H = \frac{1}{\sinh(2i\eta)}\left(H^{obc}_{XXZ}(\Delta) - \Delta\right)$$

with

$$H^{obc}_{XXZ}(\Delta) = \sum_{n=1}^{N-1} h_{XXZ}(\Delta).$$

The precondition for the Bethe ansatz is that a representation must exist, for which there is a pseudovacuum $|\mathrm{vac}\rangle$ that is an eigenstate of $\mathcal{A}(\lambda)$ and $\mathcal{D}(\lambda)$ and that is annihilated by $\mathcal{C}(\lambda)$:

$$\mathcal{A}(\lambda)|\mathrm{vac}\rangle = a(\lambda)|\mathrm{vac}\rangle,$$
$$\mathcal{D}(\lambda)|\mathrm{vac}\rangle = d(\lambda)|\mathrm{vac}\rangle,$$
$$\mathcal{C}(\lambda)|\mathrm{vac}\rangle = 0.$$

As argued before, the operator $\mathcal{C}(\lambda)$ annihilates one down-spin, whereas $\mathcal{A}(\lambda)$ and $\mathcal{D}(\lambda)$ keep the number of down-spins

constant, such that the state with all spins up is a valid pseudovacuum. The goal is now to diagonalize the transfer matrix $\tau(\lambda) = \mathcal{A}(\lambda) + \mathcal{D}(\lambda)$. Since all transfer matrices commute, $[\tau(\lambda),\tau(\mu)] = 0$, all eigenvectors are independent of λ. The eigenvalue problem reads

$$\tau(\lambda)|\Psi\rangle = \tau(\lambda)|\Psi\rangle.$$

The Bethe ansatz

$$|\Psi(\mu_1,\ldots,\mu_M)\rangle = \mathcal{B}(\mu_1)\cdots\mathcal{B}(\mu_M)|\mathrm{vac}\rangle$$

fulfills the eigenvalue problem provided that the μ_j values fulfill the Bethe equations. The proof is based on the algebraic relations among $\mathcal{A}(\lambda)$, $\mathcal{B}(\lambda)$, $\mathcal{C}(\lambda)$ and $\mathcal{D}(\lambda)$ and is described in detail in 26.

Defining the momenta p_j via

$$p_j = i\ln\frac{\mu_j}{\mu_j+\eta},$$

the Bethe equations in their logarithmic form read[41,42]

$$(N+1)p_n = \pi I_n + \Theta(p_n,-p_n) + \sum_{\substack{j=1\\ j\neq n}}^{M}\frac{\Theta(p_n,-p_j)+\Theta(p_n,p_j)}{2},$$

with $\Theta(p,q)$ being defined in (A17). The ground state for N even and $M = N/2$ corresponds to $(I_1,\ldots,I_M) = (1,3,\ldots,N-1)$. The energy eigenvalue of $H^{obc}_{XXZ}(\Delta)$ for a configuration $(p_1,\ldots,p_M)$ is obtained as

$$E^{obc}_{XXZ}(\Delta) = -2\sum_{j=1}^{M}(\Delta-\cos(p_j)).$$

APPENDIX C: ALGEBRAIC DERIVATION OF THE BETHE EQUATIONS

For completeness, we sketch here the derivation of the Bethe equations using algebraic relations. We thereby follow Korepin *et al.*[2]

The goal is to find eigenvectors of $t(\lambda) = A(\lambda) + D(\lambda)$ using algebraic relations among $A(\lambda),B(\lambda),C(\lambda)$, and $D(\lambda)$. The commutation relations that are required are

$$B(\lambda)B(\mu) = B\ (\mu)B(\lambda), \tag{C1}$$

$$A(\lambda)B(\mu) = f\ (\lambda,\mu)B(\mu)A(\lambda) + g(\lambda,\mu)B(\lambda)A(\mu), \tag{C2}$$

$$D(\lambda)B(\mu) = f\ (\mu,\lambda)B(\mu)D(\lambda) + g(\mu,\lambda)B(\lambda)D(\mu). \tag{C3}$$

Here, the abbreviations $f(\lambda,\mu) = 1/c(\mu,\lambda)$ and $g(\lambda,\mu) = -b(\mu,\lambda)/c(\mu,\lambda)$ are used.

The Bethe ansatz reads

$$|\Psi(\mu_1,\ldots,\mu_M)\rangle = B(\mu_1)\cdots B(\mu_M)|\mathrm{vac}\rangle, \tag{C4}$$

where $|\mathrm{vac}\rangle$ is a state that is an eigenvector of $A(\lambda)$ and $D(\lambda)$ with eigenvalues $a(\lambda)$ and $d(\lambda)$ and that is annihilated by $C(\lambda)$. $A(\lambda)$ applied to $|\Psi(\mu_1,\ldots,\mu_M)\rangle$ using relation (C2) yields, in principle, 2^M terms, because each commutation of $A(\lambda)$ with a $B(\mu_k)$ yields two terms and it takes M commutations to move $A(\lambda)$ from left to right. However, these two terms are not arbitrary. Both terms only perform exchange operators: the f term in (C2) exchanges operators A and B *but not* their arguments; the g term, on the other hand, exchanges operators A and B *and* their arguments. Due to this, after M commutations the following conditions must hold:

(1) Every term must contain M B's and one A.

(2) The $M+1$ coefficients $(\lambda,\mu_1,\ldots,\mu_M)$ are distributed among the M Bs and the one A.

Since all Bs commute, there are only two cases: either λ is an argument of A, in which case the term looks like

$$B(\mu_1)\cdots B(\mu_M)A(\lambda)|\mathrm{vac}\rangle, \tag{C5}$$

or λ is an argument of one of the Bs, so the term is of the form

$$B(\lambda)\prod_{j\neq n}B(\mu_j)A(\mu_n)|\mathrm{vac}\rangle \tag{C6}$$

with $n\in\{1,\ldots,M\}$. Thus, the 2^M terms can be collected into $M+1$ linearly independent terms:

$$A(\lambda)|\Psi(\mu_1,\ldots,\mu_M)\rangle = \Lambda B(\mu_1)\cdots B(\mu_M)A(\lambda)|\mathrm{vac}\rangle + \sum_{n=1}^{M}\Lambda_n B(\lambda)\prod_{j\neq n}B(\mu_j)A(\mu_n)|\mathrm{vac}\rangle.$$

What remains to be done is the calculation of the coefficients Λ and Λ_n.

Expression (C5) is obviously obtained after M commutations using the f term in (C2). The g term must not be applied, because it introduces a $B(\lambda)$. Thus

$$\Lambda = \prod_{j=1}^{M}f(\lambda,\mu_j).$$

To obtain (C6), it is convenient to rewrite the Bethe ansatz, (C4), as

$$|\Psi(\mu_1,\ldots,\mu_M)\rangle = B(\mu_n)\prod_{j\neq n}B(\mu_j)|\mathrm{vac}\rangle.$$

This is possible for all n, since all Bs commute. Since expression (C6) must not contain $B(\mu_n)$, the first commutation with $A(\lambda)$ must be performed using the g term in (C2). The expression then reads

$$g(\lambda,\mu_n)B(\lambda)A(\mu_n)\prod_{j\neq n}B(\mu_j)|\mathrm{vac}\rangle.$$

All further commutations must use the f term, because another use of the g term would introduce $B(\mu_n)$ in the expression again. Thus, the coefficients must be

$$\Lambda_n = g(\lambda,\mu_n)\prod_{j\neq n}f(\mu_n,\mu_j).$$

The application of $D(\lambda)$ to $|\Psi(\mu_1,\ldots,\mu_M)\rangle$ can be treated in a similar way using relations (C1) and (C3). Again, the application yields $M+1$ terms,

$$D(\lambda)|\Psi(\mu_1,\ldots,\mu_M)\rangle = \tilde{\Lambda}B(\mu_1)\cdots B(\mu_M)D(\lambda)|\mathrm{vac}\rangle + \sum_{n=1}^{M}\tilde{\Lambda}_n B(\lambda)\prod_{j\neq n}B(\mu_j)D(\mu_n)|\mathrm{vac}\rangle.$$

The coefficients are

$$\tilde{\Lambda} = \prod_{j=1}^{M} f(\mu_j,\lambda)$$

and

$$\tilde{\Lambda}_n = g(\mu_n,\lambda)\prod_{j\neq n} f(\mu_j,\mu_n).$$

Thus, $|\Psi(\mu_1,\ldots,\mu_M)\rangle$ is an eigenvector of $t(\lambda) = A(\lambda) + D(\lambda)$ if

$$a(\mu_n)\Lambda_n + d(\mu_n)\tilde{\Lambda}_n = 0$$

for $n = 1,\ldots,M$. These relations are the Bethe ansatz equations, which can be written in the form

$$\frac{d(\mu_n)}{a(\mu_n)} = \prod_{\substack{j=1\\ j\neq n}}^{M} \frac{c(\mu_n,\mu_j)}{c(\mu_j,\mu_n)}$$

under the assumption that $g(\lambda,\mu)$ is an odd function in the sense that $g(\lambda,\mu) = -g(\mu,\lambda)$ (as is the case for the Heisenberg model and the *XXZ* model).

The eigenvalue $\tau(\lambda)$ is obtained as

$$\tau(\lambda) = a(\lambda)\Lambda + d(\lambda)\tilde{\Lambda},$$

which can be expressed as

$$\tau(\lambda) = a(\lambda)\prod_{j=1}^{M}\frac{1}{c(\mu_j,\lambda)} + d(\lambda)\prod_{j=1}^{M}\frac{1}{c(\lambda,\mu_j)}.$$

APPENDIX D: NUMERICAL STATE APPROXIMATION

The main building block of the algorithm is the approximation of MPS $|\Psi_m\rangle$ with a fixed number of m down-spins and virtual dimension D by an MPS $|\tilde{\Psi}_m\rangle$ that also has m down-spins and virtual dimension $\tilde{D} < D$ in a way that the distance (4) between the two states is minimal. The state $|\Psi_m\rangle$ reads

$$|\Psi_m\rangle = \sum_{k_1\cdots k_N}\langle 0|\langle 0|\mathcal{A}^{k_1}\cdots\mathcal{A}^{k_N}|0\rangle|m\rangle|k_1,\ldots,k_N\rangle$$

with $\langle\alpha|\langle s|\mathcal{A}^k|\beta\rangle|s'\rangle \equiv [\mathcal{A}^k]^{\alpha s}_{\beta s'}$ and $s' = s + k$. The MPS $|\tilde{\Psi}_m\rangle$ has the same structure but may be inhomogeneous, i.e., the matrices may be site dependent:

$$|\tilde{\Psi}_m\rangle = \sum_{k_1\cdots k_N}\langle 0|\langle 0|\tilde{\mathcal{A}}_1^{k_1}\cdots\tilde{\mathcal{A}}_N^{k_N}|0\rangle|m\rangle|k_1,\ldots,k_N\rangle.$$

We obtain the starting point for the optimization by setting $|\tilde{\Psi}_m\rangle$ equal to $|\Psi_m\rangle$ and performing Schmidt decompositions successively for bonds $(1,2)$ to $(N-1,N)$, where we keep at each bond only the $\tilde{D}$ largest Schmidt coefficients. Due to the conservation of the number of down-spins, the Schmidt decomposition with respect to one bond $(j,j+1)$ can be written as

$$|\tilde{\Psi}_m\rangle = \sum_{s=0}^{m}\sum_{\gamma=0}^{\Gamma_s}\sigma_\gamma^s\left|\Phi_\gamma^s\right\rangle\otimes\left|\bar{\Phi}_\gamma^{m-s}\right\rangle.$$

Thereby, states $\{|\Phi_\gamma^s\rangle|\gamma = 1,\ldots,\Gamma_s\}$ are states acting on the left block (sites $1,\ldots,j$) with a fixed number of s down-spins. In addition, these states satisfy the orthonormality constraint $\langle\Phi_\gamma^s|\Phi_{\gamma'}^s\rangle = \delta_{\gamma\gamma'}$. In an analogous manner, $\{|\bar{\Phi}_\gamma^{m-s}\rangle|\gamma = 1,\ldots,\Gamma_s\}$ are orthonormal states acting on the right block (sites $j+1,\ldots,N$) with a fixed number of $m-s$ down-spins. The singular values corresponding to the partitioning of s down-spins in the left block and $m-s$ down-spins in the right block are $\{\sigma_\gamma^s|\gamma = 1,\ldots,\Gamma_s\}$.

The Schmidt decomposition can be obtained by transforming the MPS into the form

$$|\tilde{\Psi}_m\rangle = \sum_{k_1\cdots k_N}\langle 0|\langle 0|\cdots\tilde{\mathcal{A}}_j^{k_j}\Sigma\tilde{\mathcal{A}}_{j+1}^{k_{j+1}}\cdots|0\rangle|m\rangle|k_1,\ldots,k_N\rangle,$$

with $\tilde{\mathcal{A}}_i^k$ fulfilling the local constraints $\sum_k(\tilde{\mathcal{A}}_i^k)^\dagger\tilde{\mathcal{A}}_i^k = \mathbb{1}$ for $i = 1,\ldots,j$ and $\sum_k\tilde{\mathcal{A}}_i^k(\tilde{\mathcal{A}}_i^k)^\dagger = \mathbb{1}$ for $i = j+1,\ldots,N$. The local constraints guarantee the orthonormality of the states in the left and right blocks. Σ is a diagonal matrix containing the Schmidt coefficients. The transformation into this form is always possible due to the gauge invariance of MPS.[8]

For $i \leqslant j$, the way to meet the local constraints is by QR decompositions of the matrices $\hat{\mathcal{A}}_i^{s'}$ defined as $[\hat{\mathcal{A}}_i^{s'}]^{\alpha sk}_\beta \equiv [\tilde{\mathcal{A}}_i^k]^{\alpha s}_{\beta s'}$, successively for $i = 1,\ldots,j$: $\hat{\mathcal{A}}_i^{s'} = Q_i^{s'}R_i^{s'}$. The matrix $Q_i^{s'}$ is an appropriate replacement for $\hat{\mathcal{A}}_i^{s'}$, because the orthogonality of $Q_i^{s'}$ makes the local constraint satisfied. To keep the MPS invariant, the block-diagonal matrix R_i defined as $[R_i]^{\alpha s}_{\beta s'} \equiv [R_i^{s'}]^\alpha_\beta\delta_{ss'}$ must be used to update $\tilde{\mathcal{A}}_{i+1}^k$ to $R_i\tilde{\mathcal{A}}_{i+1}^k$. Only at the last step, $i = j$, must the update be omitted. For $i > j$, LQ decompositions are performed in an analogous manner: successively for $i = N,\ldots,j+1$, the matrices $[\hat{\mathcal{A}}_i^s]^\alpha_{\beta s'k} \equiv [\tilde{\mathcal{A}}_i^k]^{\alpha s}_{\beta s'}$ are decomposed as $L_i^sQ_i^s$. Matrices Q_i^s are then used to replace $\hat{\mathcal{A}}_i^s$ and L_i^s update $\tilde{\mathcal{A}}_{i-1}^k$ to $\tilde{\mathcal{A}}_{i-1}^kL_i$ (with $[L_i]^{\alpha s}_{\beta s'} \equiv [L_i^s]^\alpha_\beta\delta_{ss'}$). As before, the update must be omitted at the last step, $i = j+1$.

The Schmidt decomposition is now obtained by performing a singular value decomposition of the product of the "leftover" update matrices R_j^s and L_{j+1}^s: $R_j^sL_{j+1}^s = U^s\Sigma^sV^s$. U^s and V^s are unitary, as well as their block-diagonal extensions U and V, defined as $[U]^{\alpha s}_{\beta s'} \equiv [U^s]^\alpha_\beta\delta_{ss'}$ and $[V]^{\alpha s}_{\beta s'} \equiv [U^s]^\alpha_\beta\delta_{ss'}$. Because of their unitarity, they can be used to update $\tilde{\mathcal{A}}_j^k$ to $\tilde{\mathcal{A}}_j^kU$ and $\tilde{\mathcal{A}}_{j+1}^k$ to $V\tilde{\mathcal{A}}_{j+1}^k$ without spoiling the orthonormality constraint. Matrix Σ^s contains the Schmidt coefficients $\{\sigma_\gamma^s|\gamma = 1,\ldots,\Gamma_s\}$ related to the partitioning of s down-spins in the left block and $m-s$ down-spins in the right block. With the definition of Σ as $[\Sigma]^{\alpha s}_{\beta s'} \equiv [\Sigma^s]^\alpha_\beta\delta_{ss'}$, we have obtained the desired form of the MPS.

A sensible way to reduce the dimension of bond $(j,j+1)$ is to keep only the largest $\tilde{D}$ Schmidt coefficients and setting all others to 0. Thus, by defining a projector P, such that $P\Sigma P^\dagger$ is the $\tilde{D}\times\tilde{D}$ matrix containing the $\tilde{D}$ largest Schmidt coefficients and updating $\tilde{\mathcal{A}}_j^k$ to $\tilde{\mathcal{A}}_j^kP^\dagger$ and $\tilde{\mathcal{A}}_{j+1}^k$ to $P\Sigma\tilde{\mathcal{A}}_{j+1}^k$, we obtain the favored MPS with reduced bond dimension.

Performing the Schmidt decompositions with successive projections for all bonds $(1,2)$ to $(N-1,N)$ gives an MPS that is a fairly good starting point for the optimization problem, (4). A further improvement is possible by optimizing the quantity K locally, i.e., by optimizing K with respect to the matrices $\{\tilde{\mathcal{A}}_j^k|k = 0,1\}$ at one site j and keeping all other matrices constant. This has been discussed extensively in 8 and 23. The main idea is that K is a quadratic function of $\tilde{\mathcal{A}}_j^k$, such that it

can be written as

$$K = \text{const} + \sum_{kk'} (\tilde{\mathcal{A}}_j^k)^\dagger \mathcal{N}_j^{kk'} \tilde{\mathcal{A}}_j^{k'} + \sum_k (\tilde{\mathcal{A}}_j^k)^\dagger w_j^k.$$

The minimum with respect to $\tilde{\mathcal{A}}_j^k$ is achieved for those values of $\tilde{\mathcal{A}}_j^k$ solving the system of linear equations

$$\sum_{k'} \mathcal{N}_j^{kk'} \tilde{\mathcal{A}}_j^{k'} = w_j^k.$$

The matrix $\mathcal{N}_j^{kk'}$ is a function of $\tilde{\mathcal{A}}_i^k, i \neq j$, and it is equal to the identity if the constraints $\sum_k (\tilde{\mathcal{A}}_i^k)^\dagger \tilde{\mathcal{A}}_i^k = \mathbb{1}$ for $i = 1, \ldots, j-1$ and $\sum_k \tilde{\mathcal{A}}_i^k (\tilde{\mathcal{A}}_i^k)^\dagger = \mathbb{1}$ for $i = j+1, \ldots, N$. are fulfilled. These constraints, however, can always be imposed, as argued earlier. By performing the local minimization for j sweeping between 1 and N until convergence of K, the global minimum of K is (usually) obtained and we have found the optimal approximation $|\tilde{\Psi}_m\rangle$ with maximal bond dimension $\tilde{D}$ to state $|\Psi_m\rangle$.

*Corresponding author: valentin.murg@univie.ac.at

[1] H. Bethe, Z. Phys. **71**, 205 (1931).

[2] V. E. Korepin, N. M. Bogoliubov, and A. G. Izergin, *Quantum Inverse Scattering Method and Correlation Functions* (Cambridge University Press, Cambridge, 1993).

[3] N. A. Slavnov, Russ. Math. Surv. **62**, 727 (2007).

[4] I. Affleck, T. Kennedy, E. H. Lieb, and H. Tasaki, Phys. Rev. Lett. **59**, 799 (1987).

[5] I. Affleck, T. Kennedy, E. H. Lieb, and H. Tasaki, Commun. Math. Phys. **115**, 477 (1988).

[6] F. Verstraete and J. I. Cirac, Phys. Rev. B **73**, 094423 (2006).

[7] D. Perez-Garcia, F. Verstraete, M. Wolf, and J. Cirac, Quantum Inf. Comput. **7**, 401 (2007).

[8] F. Verstraete, J. I. Cirac, and V. Murg, Adv. Phys. **57**(2), 143 (2008).

[9] S. Singh, R. N. C. Pfeifer, and G. Vidal, Phys. Rev. A **82**, 050301 (2010).

[10] S. R. White, Phys. Rev. Lett. **69**, 2863 (1992).

[11] S. R. White, Phys. Rev. B **48**, 10345 (1993).

[12] F. Verstraete and J. I. Cirac, arXiv:cond-mat/0407066.

[13] V. Murg, F. Verstraete, and J. I. Cirac, Phys. Rev. A **75**, 033605 (2007).

[14] V. Murg, F. Verstraete, and J. I. Cirac, Phys. Rev. B **79**, 195119 (2009).

[15] G. Vidal, arXiv:cond-mat/0512165v2.

[16] G. Vidal, Phys. Rev. Lett. **101**, 110501 (2008).

[17] F. Verstraete, *PEPS, Matrix Product Operators and the Algebraic Bethe Ansatz, Conference on Numerical Approaches to Quantum Many-Body Systems, UCLA* (2009) [https://www.ipam.ucla.edu/publications/qs2009/qs2009_8052.ppt].

[18] H. Katsura and I. Maruyama, J. Phys. A **43**, 175003 (2010).

[19] F. C. Alcaraz and M. J. Lazo, J. Phys. A **37**, 4149 (2004).

[20] F. C. Alcaraz and M. J. Lazo, J. Phys. A **37**, L1 (2004).

[21] F. C. Alcaraz and M. J. Lazo, J. Phys. A **39**, 11335 (2006).

[22] J.-S. Caux, J. Math. Phys. **50**, 095214 (2009).

[23] V. Murg, F. Verstraete, and J. I. Cirac, Phys. Rev. Lett. **95**, 057206 (2005).

[24] F. Verstraete, J. J. García-Ripoll, and J. I. Cirac, Phys. Rev. Lett. **93**, 207204 (2004).

[25] I. V. Cherednik, Theor. Math. Phys. **61**, 977 (1984).

[26] E. K. Sklyanin, J. Phys. A **21**, 2375 (1988).

[27] V. Murg, V. E. Korepin, and F. Verstraete, arXiv:1201.5627.

[28] J. Sato, M. Shiroishi, and M. Takahashi, J. Stat. Mech.: Theory Exp. (2006) P12017.

[29] C. Gómez, M. Ruiz-Altaba, and G. Sierra, *Quantum Groups in Two-Dimensional Physics* (Cambridge University Press, Cambridge 1996).

[30] F. H. L. Essler, H. Frahm, F. Göhmann, A. Klümper, and V. E. Korepin, *The One-Dimensional Hubbard Model* (Cambridge University Press, Cambridge 2005).

[31] A. A. Zvyagin, *Finite Size Effects in Correlated Electron Models: Exact Results* (Imperial College Press, London, 2005).

[32] J. Plunkett, *An Introduction to the Algebraic Bethe Ansatz* (VDM Verlag, Saarbrücken, Germany, 2009).

[33] F. Verstraete, D. Porras, and J. I. Cirac, Phys. Rev. Lett. **93**, 227205 (2004).

[34] L. Hulthén, Arkiv. Mat. Astron. Fys. **26A**, No. 11 (1938).

[35] M. Karbach and G. Müller, Comput. Phys. **11**, 36 (1997).

[36] M. Karbach, K. Hu, and G. Müller, arXiv:cond-mat/9809163v1.

[37] M. Karbach, K. Hu, and G. Müller, arXiv:cond-mat/0008018v1.

[38] C. N. Yang and C. P. Yang, Phys. Rev. **150**, 321 (1966).

[39] R. Orbach, Phys. Rev. **112**, 309 (1958).

[40] N. Kitanine, K. K. Kozlowski, J. M. Maillet, G. Niccoli, N. A. Slavnov, and V. Terras, J. Stat. Mech. (2007) P10009.

[41] M. Gaudin, Phys. Rev. A **4**, 386 (1971).

[42] F. C. Alcaraz, M. N. Barber, M. T. Batchelor, R. J. Baxter, and G. R. W. Quispel, J. Phys. A **20**, 6397 (1987).